ROS-activated ATM-dependent phosphorylation of cytoplasmic substrates identified by large scale phosphoproteomics screen

Kozlov, Sergei V; Waardenberg, Ashley J; Engholm-Keller, Kasper; Arthur, Jonathan W; Graham, Mark E; Lavin, Martin F

Published in:
Molecular and Cellular Proteomics

DOI:
10.1074/mcp.M115.055723

Publication date:
2016

Document version
Publisher's PDF, also known as Version of record

Citation for pulished version (APA):
Kozlov, S. V., Waardenberg, A. J., Engholm-Keller, K., Arthur, J. W., Graham, M. E., & Lavin, M. F. (2016). ROS-activated ATM-dependent phosphorylation of cytoplasmic substrates identified by large scale phosphoproteomics screen. Molecular and Cellular Proteomics, 15(3), 1032-1047. DOI: 10.1074/mcp.M115.055723

Research

Reactive Oxygen Species (ROS)-Activated ATM-Dependent Phosphorylation of Cytoplasmic Substrates Identified by Large-Scale Phosphoproteomics Screen*[S]

Sergei V. Kozlov‡, Ashley J. Waardenberg§, Kasper Engholm-Keller¶‖, Jonathan W. Arthur§, Mark E. Graham¶, and Martin Lavin‡**

Ataxia-telangiectasia, mutated (ATM) protein plays a central role in phosphorylating a network of proteins in response to DNA damage. These proteins function in signaling pathways designed to maintain the stability of the genome and minimize the risk of disease by controlling cell cycle checkpoints, initiating DNA repair, and regulating gene expression. ATM kinase can be activated by a variety of stimuli, including oxidative stress. Here, we confirmed activation of cytoplasmic ATM by autophosphorylation at multiple sites. Then we employed a global quantitative phosphoproteomics approach to identify cytoplasmic proteins altered in their phosphorylation state in control and ataxia-telangiectasia (A-T) cells in response to oxidative damage. We demonstrated that ATM was activated by oxidative damage in the cytoplasm as well as in the nucleus and identified a total of 9,833 phosphorylation sites, including 6,686 high-confidence sites mapping to 2,536 unique proteins. A total of 62 differentially phosphorylated peptides were identified; of these, 43 were phosphorylated in control but not in A-T cells, and 19 varied in their level of phosphorylation. Motif enrichment analysis of phosphopeptides revealed that consensus ATM serine glutamine sites were overrepresented. When considering phosphorylation events, only observed in control cells (not observed in A-T cells), with predicted ATM sites phosphoSerine/phosphoThreonine glutamine, we narrowed this list to 11 candidate ATM-dependent cytoplasmic proteins. Two of these 11 were previously described as ATM substrates (HMGA1 and UIMCI/RAP80), another five were identified in a whole cell extract phosphoproteomic screens, and the remaining four proteins had not been identified previously in DNA damage response screens. We validated the phosphorylation of three of these proteins (oxidative stress responsive 1 (OSR1), HDGF, and ccdc82) as ATM dependent after H_2O_2 exposure, and another protein (S100A11) demonstrated ATM-dependence for translocation from the cytoplasm to the nucleus. These data provide new insights into the activation of ATM by oxidative stress through identification of novel substrates for ATM in the cytoplasm. ***Molecular & Cellular Proteomics 15: 10.1074/mcp.M115.055723, 1032–1047, 2016.***

Ataxia-telangiectasia (A-T) is a rare, human, autosomal recessive disease involving complex multisystem defects characterized by progressive neurological dysfunction, immunological abnormalities, growth retardation, and cancer predisposition (1), caused by mutations in the ataxia-telangiectasia, mutated (ATM)[1] protein. ATM is a protein kinase in-

From the ‡University of Queensland Centre for Clinical Research, University of Queensland, Royal Brisbane & Women's Hospital Campus, Herston, Brisbane, QLD 4029 Australia; §Bioinformatics Unit, Children's Medical Research Institute, University of Sydney, 214 Hawkesbury Road, Westmead, NSW, 2145, Australia; ¶Synapse Proteomics Group, Children's Medical Research Institute, University of Sydney, 214 Hawkesbury Road, Westmead, NSW, 2145, Australia; ‖Department of Biochemistry and Molecular Biology, University of Southern Denmark, DK-5230 Odense M, Denmark

Received September 21, 2015, and in revised form, December 8, 2015

Published, MCP Papers in Press, December 23, 2015, DOI 10.1074/mcp.M115.055723

Author contributions: S.V.K., A.J.W., M.E.G., and M.F.L. designed the research; S.V.K., A.J.W., K.E., and M.E.G. performed the research; K.E. and M.E.G. contributed new reagents or analytic tools; S.V.K., A.J.W., J.W.A., M.E.G., and M.F.L. analyzed data; and S.V.K., A.J.W., and M.F.L. wrote the paper.

[1] The abbreviations used are: ATM, ataxia-telangiectasia mutated protein kinase; ATR, ataxia telangiectasia and Rad3-related protein kinase; SQ, Serine followed by Glutamine motif; TQ, Threonine followed by Glutamine motif; p(S/T), Q phosphoSerine/phosphoThreonine followed by Glutamine – ATM/ATR phosphorylation motif; DMEM, Dulbecco's modified Eagle medium; RPMI 1640, Roswell Park Memorial Institute 1640 medium; HBSS, Hank's Balanced Salt Solution; PBS, Phosphate buffered saline; FCS, fetal calf serum; CERI, NE-PER Cytoplasmic Extraction Reagent I; MS/MS, tandem mass spectrometry; SILAC, stable isotope labeling by amino acids in cell culture; LTQ, Linear trap quadropole; PTM, post translational modification; RP-HPLC, reversed-phase high performance liquid chromatography; IMAC, Immobilized metal affinity chromatography; SIMAC, sequential elution from IMAC; HILIC, Hydrophilic Interaction Liquid chromatography; TEAB, Triethylammonium bicarbonate; TFA, Trifluoroacetic acid; TiSH, TiO2–SIMAC–HILIC phosphoproteomics strategy; FDR, False discovery rate; IF, immunofluorescence; IPA, Ingenuity Pathway Analysis; PAAG,Polyacrylamide gel; DDR, DNA

volved in multiple aspects of cellular metabolism, such as response to genotoxic stress, cell cycle control, and maintaining genetic stability (2, 3). The ATM protein plays a role in phosphorylating a regulatory cascade of proteins controlling cell cycle progression, DNA repair, transcription, and apoptosis, as well as signal transduction pathways responding to oxidative stress (4). ATM is rapidly activated in the presence of DNA double strand breaks, yet the mechanism of ATM kinase activation remains poorly understood. This activation is dependent on the presence of the Mre11/Rad50/NBN (MRN) complex (5). Bakkenist and Kastan (6) proposed a model for ATM activation, where rapid intermolecular autophosphorylation in response to DNA damage caused dissociation of inactive ATM dimers to form active monomers.

It now seems likely that multiple autophosphorylation sites are involved in ATM activation (7, 8). However, the importance of autophosphorylation in mice is less clear since mutations that abolish the autophosphorylation sites do not appear to interfere with the activation of ATM. ATM kinase can also be activated by oxidative stress in the absence of DNA damage, independent of MRE11-RAD50-NBN complex, but involving autophosphorylation (9). In this case the active form of ATM is not a monomer but rather a disulfide-linked, covalent dimer, and the suite of downstream substrates appears to be more limited than that activated by DNA double strand breaks (5). More recently, it has been reported that the peroxisome import receptor protein, PEX5, binds ATM and localizes it to peroxisomes (10). ATM had previously been localized to this organelle (11). In the latest report, ATM was shown to phosphorylate PEX5 at Ser^{141}, which promotes its ubiquitylation to induce autophagy of peroxisomes (pexophagy). In addition, activation of ATM should not be viewed in isolation since a complex set of relationships exist between all DNA-damage-inducible kinases: ATM, ATR, DNA-PK, and SMG1. Certain DNA damage stimuli can promote transphosphorylation of autophosphorylation sites, as was shown in the case of ATR-ATM and ATM-DNA-PK kinases, and there is also evidence for cross-regulation between these kinases (12–14). Furthermore, protein phosphatases PP5, PP2A, PP2C and WIP1 have been implicated in the regulation of ATM kinase activity (15–17). Similarly, regulation of ATM kinase activity by acetylation via interaction with acetyltransferases Tip60/KAT5 (18, 19) and hMOF1 has been reported (20).

To understand these complex signaling networks, numerous traditional and proteomic approaches have been utilized to identify ATM signaling pathways and substrates (reviewed in (4)). However, there have been some limitations in phosphoproteomic screens used to investigate ATM-dependent signaling pathways. The bulk of these studies employed different cancer cell lines, and A-T cells had not been included. Phospho-specific antibodies against ATM/ATR substrates (p(S/T)Q antibodies) were used to identify potential candidates in human embryonic kidney 293T cells (21) or HeLa cells (22) after DNA damage. Subsequent screens again utilized cancer cell lines in combination with the ATM inhibitor KU55933 (23, 24). A quantitative phosphoproteomic SILAC-based approach used U2OS cells, etoposide, and radiation as DNA-damaging agents (25) or lymphoblastoid cells treated with x-ray radiation (26). A number of ATM/ATR signaling events have also been identified in large-scale phosphoproteomic screens of basic cellular functions, *e.g.* mitosis (27). Clearly, there exists a need to investigate ATM-dependent signaling pathways using primary control and A-T cells.

While proteomics screens have created a wealth of information on ATM-dependent DNA damage signaling caused by DNA double strand breaks, it is apparent that they do not extensively address important functions of ATM kinase outside of the nucleus. Several reports provide evidence for a cytoplasmic localization of ATM (11, 28–30), and this may be particularly relevant to a role for ATM in responding to oxidative damage in the brain. ATM can be activated by a variety of stimuli, including oxidative stress, a mechanism not involving DNA double strand breaks (9). It is not clear at the moment to what extent overlapping sets of substrates are involved in ATM signaling in response to DNA double strand breaks compared with ATM signaling in response to oxidative stress

damage response; HMGA1, high mobility group AT-hook 1 protein; UIMCI/RAP80, BRCA1-A complex subunit RAP80 protein; HDGF, Hepatoma-derived growth factor; Ccdc82, Coiled-coil domain-containing protein 82; OSR1, Oxidative Stress Responsive 1 protein kinase; Mre11, Double-strand break repair protein MRE11A (Meiotic recombination 11 homolog 1); Rad50, DNA repair protein RAD50; NBN, Nibrin, Nijmegen breakage syndrome protein 1; MRN, MRE11-RAD50-NBN complex; PEX5, Peroxisomal targeting signal 1 receptor; DNA-PK, DNA-dependent protein kinase, catalytic subunit; SMG1, Serine/threonine-protein kinase SMG1; PP5, Serine/threonine-protein phosphatase 5; PP2A, Protein phosphatase 2A; PP2C, Protein phosphatase 2C; WIP1, Protein phosphatase 1D; Tip60/KAT5, Histone acetyltransferase KAT5; hMOF, Histone acetyltransferase KAT8; KU55933, 2-(4-Morpholinyl)-6-(1-thianthrenyl)-4H-pyran-4-one; U2OS,human osteosarcoma cell line; LKB1,Serine/threonine-protein kinase STK11; AMPK,AMP-activated protein kinase; TSC2,Tuberin; mTORC1, mammalian target of rapamycin complex 1; Akt, Protein kinase B; 4E-BP1, Eukaryotic translation initiation factor 4E-binding protein 1; NEMO,NF-kappa-B essential modulator; TRAF6, TNF receptor-associated factor 6; Hsp27, Heat shock protein beta-1; HIF1a, Hypoxia-inducible factor 1-alpha; VAMP2, Vesicle-associated membrane protein 2; KAP1, Transcription intermediary factor 1-beta; SMC1, Structural maintenance of chromosomes protein 1; H2AX, Histone H2AX; TCEAL3/6, Transcription elongation factor A protein-like 3; ATE1, Arginyl-tRNA–protein transferase 1; METTL16, Methyltransferase-like protein 16; WNK1, Serine/threonine-protein kinase WNK1; STRING, Search Tool for the Retrieval of Interacting Genes/Proteins database; EEA1, Early endosome antigen 1; MAPK1/ERK2, Mitogen-activated protein kinase 1; MAPK3/ERK1, Mitogen-activated protein kinase 3; PRAS40, Proline-rich AKT1 substrate 1; RPTOR, Regulatory-associated protein of mTOR; UREB1, E3 ubiquitin-protein ligase HUWE1; UFD1L, Ubiquitin fusion degradation protein 1 homolog; ATXN3, Ataxin-3; MON1, Vacuolar fusion protein MON1 homolog A; TGFβ, Transforming growth factor beta; PPM1G, Protein phosphatase 1G; NKCC1, Solute carrier family 12 member 2 protein; NKCC2, Na-K-2Cl cotransporter; NCC, sodium-chloride symporter.

(31, 32). Indeed, a long-standing debate in the A-T field is the relative contributions of DNA double strand breaks and oxidative stress to neurodegeneration and neuronal cell death (33, 34). It was previously demonstrated that kainic acid can activate ATM in the cytoplasm of neurons of the cerebral cortex without creating any detectable DNA damage (35). It seems plausible that this action of kainic acid is mediated by signaling through reactive oxygen species (ROS). Resveratrol has been demonstrated to activate ATM in the presence of ROS (36), suggesting that a phosphoproteomic screen using resveratrol as an inducer of autophagy (37) potentially uncovers ATM-dependent signaling events independent of DNA damage. In addition, ATM signaling has been shown to engage the LKB1-AMPK pathway to activate TSC2 in order to suppress mTORC1 signaling in response to oxidative stress (38). ATM localization to endosomes (39), peroxisomes and as yet unidentified cytoplasmic vesicles (11, 40) and mitochondria (41) have all been demonstrated. A number of ATM cytoplasmic substrates and interacting proteins have been identified by a variety of traditional biochemical approaches (β-adaptin, 4E-BP1, B56γ-PP2A, PP2A/C, LKB1, Akt, NEMO, TRAF6, Hsp27, HIF1a, VAMP2) (28, 42–50). However, investigation of the global response of normal and A-T cells to oxidative stress in the cytoplasm is lacking.

Here, we systematically investigated ATM-dependent signaling events induced by hydrogen peroxide in fibroblasts derived from normal individuals and A-T patients using a quantitative phosphoproteomics approach. First, we addressed the action of ATM kinase in primary cells from A-T patients, which provided us with a unique opportunity for the first time to investigate ATM/ATR-dependent signaling pathways in a diseased state. Secondly, it was possible to directly compare the action of an ATM kinase activating stimulus (H_2O_2) in the physiological context of nontransformed, nonimmortalized primary control and A-T fibroblasts. The quantitative phosphoproteomics approach enabled identification of 9,612 phosphorylation sites, which were analyzed statistically. Phosphosites that were changing their level of activity and/or were lost in the A-T cells were identified as preferentially enriched in the ATM consensus (S/T)Q sites (51), using an unbiased method. These proteins were also preferentially enriched for the cytoplasm based on known protein localization. Of these phosphosites identified, we validated the phosphorylation of three of these proteins (OSR1, HDGF, and ccdc82) as ATM-dependent after H_2O_2 exposure and another protein (S100A11) as ATM dependent for translocation from the cytoplasm to the nucleus. These data provide new insights into the activation of ATM by oxidative stress through identification of novel substrates for ATM in the cytoplasm.

EXPERIMENTAL PROCEDURES

Cell Culture and Treatments—Cell cultures of primary neonatal foreskin fibroblasts (NFF) were established from normal healthy individuals. Primary cultures of A-T fibroblasts (AT34 ABR) were established from skin biopsies of A-T patients obtained in the A-T Clinic (Royal Children's Hospital, Brisbane, Australia). All procedures were approved by the Children's Health Queensland Hospital and Health Service Human Research Ethics committee. Fibroblasts cultures were grown to 80–90% confluence in DMEM supplemented with penicillin, streptomycin, and either 10% FCS for the normal fibroblasts or 15% FCS in the case of the A-T fibroblasts. Lymphoblastoid cell lines (LCL) were established from a normal healthy individual (C3ABR) and an A-T patient (AT25ABR) by Epstein–Barr virus immortalization. The lymphoblastoid cell lines were cultured in RPMI 1640 medium with 10% fetal calf serum, 100 units/ml penicillin, and 100 units/ml streptomycin (Life Technologies).

All irradiations were performed at room temperature using a Gammacell 40 Exactor research irradiator (1 Gy/min, MDS Nordion, Canada). Treatment of cells with 0.5 mM hydrogen peroxide was performed in the modified media described in (52). Cell monolayers were quickly washed with warm PBS, then warm HBSS, supplemented with 2 mM GlutaMAX™ (Life Technologies, Scoresby, VIC, Australia) and D-glucose (1 g/l) were added to the flasks to produce "untreated" samples. Hank's Balanced Salt solution/GlutaMax/glucose also containing 0.5 mM hydrogen peroxide was added to flasks to produce "H_2O_2-treated" samples. Flasks were incubated for 30 min, and cells were quickly rinsed with warm PBS, harvested by detachment using TrypLE cell-dissociation enzymes (Invitrogen Scoresby, VIC, Australia), and immediately subjected to subcellular fractionation (below). Biological replicates of NFF and A-T fibroblasts at early passage numbers were prepared for phosphoproteomics analysis in independent experiments.

Experimental Design and Statistical Rationale—Our experimental design to differentiate between ATM-dependent and ATM-independent H_2O_2 phospho-signaling involved collection of samples from independent experiments. Cytoplasmic extracts from untreated and H_2O_2 treated normal human fibroblasts were collected from four independent experiments. Similarly, cytoplasmic extracts from untreated and H_2O_2 treated A-T fibroblasts were collected from three independent experiments. The number of independent experiments was chosen to be at least three to allow a robust statistical analysis to be conducted on the data. Replicate 1 from the normal human fibroblasts experiment was from an initial test experiment and also included in the analysis to maximize on available data.

Subcellular Fractionation of Fibroblasts for Phosphoproteomics—A subcellular fractionation procedure employing NE-PER™ Nuclear and Cytoplasmic Extraction kit (ThermoScientific Scoresby, Vic, Australia) was used for isolating cytoplasmic and nuclear protein fractions as described by the manufacturer. Briefly, collected cell pellets were resuspended by gentle pipetting in chilled cytoplasmic extraction reagent I buffer supplemented with protease (50x Complete inhibitor (Roche) and 1 mM PMSF), phosphatase inhibitors (1 mM Na_3VO_4, 10 mM NaF, 10 mM Na_2MoO, 5 nM okadaic acid, 20 μM cantharidin, 10 mM β-glycerophosphate) and 1 mM DTT and processed to obtain cytoplasmic extracts. Nuclear extracts were prepared and kept at −80 °C for signaling experiments. Experimental replicates ($n = 2$ or 3) of cytoplasmic extracts were pooled and processed as described in the "Sample Preparation for Phosphoproteomics" section.

Sample Preparation for Phosphoproteomics—Protein concentration in extracts was measured by BioRad DC™ protein assay, and cytoplasmic extracts were immediately precipitated with five volumes of ice-cold acetone–ethanol–acetic acid (50:50:0.1) mixture at −20 °C overnight. Precipitated proteins were recovered by centrifugation at 20,000 *g* for 1 h at +4 °C. Pellets were washed with 80% cold ethanol and dried under a gentle stream of nitrogen. Dried proteins were dissolved in fresh 8 M urea-0.1 M ammonium bicarbonate, reduced with 10 mM DTT, and alkylated with 40 mM iodoacetic acid. Proteins were digested with LysC/trypsin (1:100 mixture) (Pro-

mega Alexandria, NSW, Australia) using a modified manufacturer's protocol. LysC digestion was performed overnight at +37 °C using an Eppendorf thermomixer. Samples were diluted 1:8 with 0.1 M ammonium bicarbonate and an additional amount of trypsin (20 μg) was added to samples. Trypsin digestion was extended by incubating samples overnight with shaking at +37 °C. Trifluoroacetic acid (TFA) was added to the samples to 1% final concentration and digests were clarified by centrifugation at 16,000 *g* for 10 min. LysC/trypsin digests of cytoplasmic proteins were purified on 360 mg Sep-Pak C18 Plus Short cartridges (Waters Rydalmere, NSW, Australia). Peptides were eluted with 50% acetonitrile, concentrated using a GenVac EZ-2 vacuum evaporator, and the relative concentration of peptides was measured using a NanoDrop 2000c spectrophotometer (Thermo Fisher Scientific). Desalted peptides were frozen at −80 °C. Equal amounts (~1 mg) of purified peptides were used in duplex stable isotope dimethyl labeling as described (53, 54). Briefly, peptides were adjusted to 125 mM triethylammonium bicarbonate and peptides were either labeled with "light" formaldehyde (CH_2O) and cyanoborohydride ($NaBH_3CN$) or with "heavy" deuterium-containing formaldehyde ($C[^2H]_2O$) and cyanoborohydride ($NaB[^2H]_3CN$) in a total volume of 200 μl for 30 min. The labeling reactions were quenched by adding 25% ammonia solution (NH_4OH) and then acidified with formic acid. The reaction volume was reduced by evaporation. The efficiency of the derivatization was confirmed by LC-MS/MS (see below) to be greater than 95% before the "light" and "heavy" samples were mixed.

Phosphopeptides in the labeled mixtures were enriched using methods similar to those described previously (55, 56). Briefly, samples in 50% acetonitrile/0.1% TFA were applied to Fe^{3+} immobilized metal affinity chromatography beads (PhosSelect, Sigma Castle Hill, NSW, Australia) and washed in the same solution. The peptides that did not bind, primarily nonphosphopeptides, were kept for later analysis. The monophosphorylated peptides were eluted using 20% acetonitrile/1% TFA. The multiphosphorylated peptides were eluted in a high pH solution (20% acetonitrile with 20% ammonium hydroxide solution (29% ammonia in water)). Monophosphorylated peptides were further fractionated using TiO_2 and hydrophilic interaction liquid chromatography chromatography. Monophosphorylated peptides were applied to TiO_2 beads in a solution of 5% TFA 80% acetonitrile, washed in 50% acetonitrile/5% TFA, and eluted with high pH solution. The eluate was immediately concentrated by evaporation and adjusted to the starting conditions of HILIC chromatography (90% acetonitrile/0.1% TFA). HILIC separation was performed using a Dionex UltiMate3000 nano HPLC system (Thermo Fisher Scientific). The monophosphorylated-peptide-enriched sample was then loaded onto a TSKgel Amide-80 HILIC 1 mm × 250 mm column (Tosoh Bioscience, Tokyo, Japan) using gradient elution from 90% ACN, 0.1% TFA to 60% ACN, 0.1% TFA for 35 min at 50 μl/min. Fractions were collected in a 96-well plate, evaporated by vacuum centrifugation, and redissolved in 5 μl of 0.1% formic acid. Ten percent of the nonphosphopeptides, the single multiphosphopeptide fraction, and the multiple monophosphopeptide fractions were analyzed separately by LC-MS/MS.

LC/MS/MS Analysis—Analysis of peptide fractions was performed using a Dionex UltiMate 3000 nanoLC system and an LTQ Orbitrap Velos mass spectrometer (Thermo Fisher Scientific). Each 5 μl fraction was loaded at 400 nl/min of 100% phase A (0.1% formic acid in water) for 20 min onto a 35 cm × 75 μm inside diameter column packed with ReproSil-Pur 120 C18-AQ 3 μm beads (Dr. Maisch Ammerbuch-Entringen, Germany). The column was heated to 45 °C. The gradient was from 2% phase B (0.1% formic acid, 9.99% water, and 90% acetonitrile) to 30% phase B in 152 min and then to 99% phase B in 5 min. During each cycle of data-dependent MS detection, the seven most-intense ions within *m/z* 300–1,500 above 500 counts in a 30,000 resolution Orbitrap MS scan were selected for fragmentation and detection in an Orbitrap MS/MS scan at 7,500 resolution. Other MS settings were: isolation width, 1.5 units; normalized collision energy, 42; activation time, 0.1 ms; Fourier transform first *m/z*, 140; Fourier transform master scan preview was enabled; monoisotopic precursor selection was enabled (unassigned charge state and charge state 1 rejected); predict ion injection time was enabled; dynamic exclusion was for 20 s with 10 ppm mass width; Orbitrap target was 1,000,000 counts for a maximum of 500 ms for MS scans and a target of 50,000 counts for a maximum of 300 ms for MS/MS scans.

Bioinformatics Analysis—The raw MS files were processed using MaxQuant 1.3.0.5 (57) (Max Planck Institute of Biochemistry) and the human reference proteome from UniProtKB (UP000005640, downloaded 9 July 2014, 68,049 entries). Peptides were assumed to have resulted from trypsin cleavage, including [K/R]/P cleavages, with a maximum of three missed cleavages. All other MaxQuant settings were default except for the following: variable modifications were phosphorylation (STY), acetyl (protein N-term), deamidation (NQ), oxidation (M), carbamidomethyl (C), dioxidation (C), and trioxidation (C), the minimum peptide length was 6, maximum labeled amino acids was 5, minimum peptide score was 40. The normalized ratios, together with phosphopeptide and protein annotations in the "Phospho (STY) sites.txt" output file, were exported for further analysis in R, version 3.1.1 (The R Foundation). Phosphopeptides not containing sites with a localization score ≥ 0.75 were excluded from further analysis. The mass spectrometry proteomics data have been deposited to the ProteomeXchange Consortium (58) via the PRIDE partner repository with the dataset identifier PXD002850.

Normalization and Rank Product Analysis—We generated four sets using the nonparametric rank product method (59) based on how many times a phosphopeptide was reported across independent experiments. No thresholding based on the magnitude of change in phosphorylation level was performed; however, phosphopeptides not passing a false discovery rate of 0.20 were discarded after statistical analysis (see below). If phosphopeptides were present in at least two A-T and two control samples, we deemed this set suitable for a two-class comparison, *i.e.* direct comparison of phosphorylation levels (Set 1). For two-class comparisons the rank product method can be sensitive to insufficiently normalized data due to the determination of ratios between contrasts prior to ranking (59). Therefore, for Set 1, data were $\log_2$ transformed, followed by quantile normalization assuming missing values were missing at random (60). Missing value imputation was then undertaken using the k-nearest neighbor method (KNNimpute) with k = 10 (61) and data iteratively reweighted using surrogate variable analysis (SVA) (62). This improved separation of A-T and NFF samples as observed using unsupervised principle component analysis (Supplemental Fig. 5 and Fig. 4*B*).

To test for cases where phosphorylation was preferentially detected, we employed a single class test (Sets 2–4). Normalized ratios from MaxQuant were converted to ranks, and the rank products were directly calculated from replicates. Here "preferentially" is defined as present in at least two of three samples for A-T and three of four samples for NFF but not detected in at least two samples of their respective contrast samples. Set 4 indicated the peptides commonly phosphorylated in both A-T and NFF cells, *i.e.* not differentially phosphorylated, but indeed phosphorylated. The overall schema is represented in Fig. 3 and summarized below:

1) detected in A-T and control cell lines ($n \geq 2$) and differentially phosphorylated
2) regulated phosphorylation detected preferentially in A-T cells ($n \geq 2$)
3) regulated phosphorylation detected preferentially in control cells ($n \geq 3$)
4) similarly regulated phosphorylation detected in both A-T and control cell lines

p values and false discovery rates (FDR) were then determined using the rank product method implemented in the RankProd R package (version 2.34) using 1,000 permutations (63). We used an FDR threshold of 0.20 to define significant phosphorylated peptides in each set. If a phosphopeptide for Set 1 was present in Sets 2–4, it was removed after the FDR calculation since it was already categorized as differentially phosphorylated according to our criteria, while maintaining the maximum number of phosphopeptides for FDR calculation. This resulted in a total of 101 phosphopeptides comprising 19, 17, 43, and 22 peptides for Sets 1, 2, 3, and 4, respectively. When analyzing proteins, we extracted the leading protein annotation for further analysis.

Gene Ontology Enrichment—Gene ontology (GO) enrichment of cytoplasmic and nuclear terms was performed using the Database for Annotation Visualization and Integrated Discovery database (64). Analysis of the "cytoplasm" and "nuclear" term associated with the identified proteins from the "SP_PIR_KEYWORDS" ontology were compared and fold enrichment (also known as the odds ratio) reported. Inputs were the leading protein annotations, and the analysis was conducted with the species set to *Homo sapiens* and all other parameters set to their default value (default background is the whole genome). The *p* values reported were derived from Database for Annotation Visualization and Integrated Discovery gene ontology charts and corresponded to a modified Fisher's Exact Test.

Motif Enrichment Analysis—Phosphopeptides identified in Sets 1–4 were tested for motif overrepresentation using Motif-x (65). Input sequences were centered on the modification site and trimmed to 13 amino acids. A background sequence set representing all 6,650 phosphopeptides identified ($p \geq 0.75$) was generated for analysis. Central characters "S" and "T" were analyzed separately and motifs were considered enriched at $p < 0.01$. Motifs with greater than two foreground hits were reported.

Comparison to Previously Published Proteomics Data—Briefly, Beli *et al.* (25) induced DNA damage via ionizing radiation (IR) for 1 h or etoposide treatment for 24 h and compared with nontreated controls. SILAC labeling was performed using whole-cell fractions and final ratios determined using MaxQuant. Nonthresholded data from MaxQuant were downloaded as per Table S1 from the Beli *et al.* 2012 publication for comparison. Two tables were subsequently generated for comparison to etoposide and IR data separately. All comparisons performed used the "Modified.Sequence" string reported by MaxQuant for each peptide identified.

Cell Extracts, ATM Immunoprecipitation, and ATM MS Analysis—Total cell extracts were prepared by lysing cells in Nonidet P-40 lysis buffer containing phosphatase and protease inhibitors (66). Sheep polyclonal ATM antibodies were used to immunoprecipitate ATM protein, separate it on biphasic 5%/12% SDS-polyacrylamide gels, and transfer to nitrocellulose membrane as described (7). ATM2C1, phospho-S367 ATM, phospho-S1981 ATM, and phospho-S2996 ATM antibodies were used to probe membranes sequentially with stripping between each step. ATM immunoprecipitations were scaled up to obtain ATM protein for mass spectrometry analysis. Identification of ATM phosphorylation sites by MS was performed essentially as described in (8).

Immunoblotting, Immunoprecipitation, and Antibodies—For immunoblotting, 50 μg of cell extracts were electrophoresed on NuPAGE 4–12% Bis-Tris mini gels and transferred to nitrocellulose membranes (Amersham Biosciences Parramatta, NSW, Australia). Membranes probed with antibodies were visualized with the Western Lightning PLUS ECL substrate (Perkin Elmer Melbourne, VIC, Australia). For immunoprecipitation of proteins phosphorylated on p(S/T)Q motifs, total cellular extracts prepared using Nonidet P-40 lysis buffer were immunoprecipitated with a mixture of phospho (S/T) ATM/ATR substrate rabbit polyclonal and phospho ATM/ATR substrate (SQ) rabbit monoclonal antibodies. Immunoprecipitates were separated on NuPAGE 4–12% Bis-Tris mini gels and transferred to nitrocellulose membranes. Membranes were stained with PonceauS and scanned to estimate immunoprecipitation efficiency and loading. Membranes were blocked with 5% skim milk powder in TBS/0.1% Tween20 and probed with antibodies against candidate proteins identified in the phosphoproteomics screen. Membranes were stripped of antibodies by incubation in 62.5 mM Tris-HCl (pH 6.8), 2%SDS, and 100 mM β-mercaptoethanol at +60C for 30 min. Membranes were washed in PBS-Tween, reblocked, and incubated with primary antibody.

ATM-specific sheep antibodies, pS367-ATM, and pS2996-ATM rabbit antibodies were prepared as described earlier (7, 8). ATM 2C1 mouse monoclonal and anti-DNAPKcs (phospho S2056) rabbit polyclonal antibodies were from Abcam (Melbourne, VIC, Australia). Anti-DNA-PK mouse monoclonal antibodies were from Calbiochem (Merck Millipore, Bayswater, VIC, Australia). ATM (pS1981) rabbit monoclonal, Mre11–2D7 mouse monoclonal, phospho-S957 SMC1 rabbit monoclonal antibodies were from GeneTex (Irvine, CA, USA). Phospho-ATR (Ser428) phospho (S/T) ATM/ATR substrate rabbit polyclonal, phospho ATM/ATR substrate (SQ) rabbit monoclonal, phospho-S15 p53 rabbit polyclonal, and phospho-T68 Chk2 rabbit polyclonal antibodies were from Cell Signaling Technology (Genesearch Pty Ltd,Arundel,QLD, Australia). KAP1 rabbit polyclonal, phospho-S824 KAP rabbit polyclonal, Nbs1 rabbit polyclonal, phospho-S343 Nbs1 rabbit polyclonal, and SMC1 rabbit polyclonal antibodies were from NOVUS Biologicals (Noble Park North, VIC, Australia). ATR N-19 goat polyclonal and p53 (Pab 1801) mouse monoclonal antibodies were from Santa-Cruz Biotechnology (VWR International, Murarrie,QLD, Australia). Rad50–2C6 mouse monoclonal, γ-H2AX (pS139) mouse monoclonal, and Chk2 rabbit polyclonal antibodies were from Merck Millipore. OSR1 rabbit polyclonal, S100A11 rabbit polyclonal, HDGF rabbit polyclonal, ccdc82 rabbit polyclonal, ATE1 rabbit polyclonal, TCEAL3/6 rabbit polyclonal, and METTL16 rabbit polyclonal antibodies were from One World Labs (San Diego, CA, USA).

IF Microscopy—Saponin permeabilization technique was used for Immunofluorescence microscopy of cytoplasmic proteins. Briefly, early passage control and A-T fibroblasts were seeded on glass round coverslips, treated with 0.5 mM H_2O_2 for 30 min in a medium used for preparation of extracts in phosphoproteomics experiments (HBSS: glucose:GlutaMAX™). Cells were fixed with 4% paraformaldehyde in cytoskeletal buffer for 15 min, permeabilized with 0.2% saponin in cytoskeletal buffer for 10 min and blocked with 0.5% BSA/5% FCS in PBS. The following antibodies were used for immunofluorescence microscopy: S100A11 rabbit polyclonal (One World Labs), anti-EEA1 mouse monoclonal (BD Transduction Laboratories North Ryde, NSW, Australia), and γH2AX (pS139) mouse monoclonal (Merck Millipore). Coverslips were incubated with S100A11 (1/100) and EEA1 (1/250) antibodies overnight at +4 °C in 0.1% saponin/0.5% BSA/5% FCS/PBS. Coverslips were washed with PBS and incubated with α-mouse-Alexa594 (highly-crosslinked), and α-rabbit-Alexa488 (highly cross-linked) (Life Technologies) secondary antibodies at room temperature for 1 h. For detection of γH2AX foci, cells were permeabilized with 0.5% Triton X-100 in cytoskeletal buffer for 10 min and then processed as described above using γH2AX antibody (1/1,000). Cells were stained with DAPI, coverslips mounted in ProLong® Gold antifade mountant (Life Technologies), and imaged on Zeiss AxioImager M1 fluorescent microscope equipped with Axiocam503 mono camera using x63 oil lens. Images were processed using ZEN software (Zeiss North Ryde, NSW, Australia).

RESULTS

Oxidative Stress Induces ATM Autophosphorylation at Multiple Sites—Autophosphorylation of ATM can be induced by

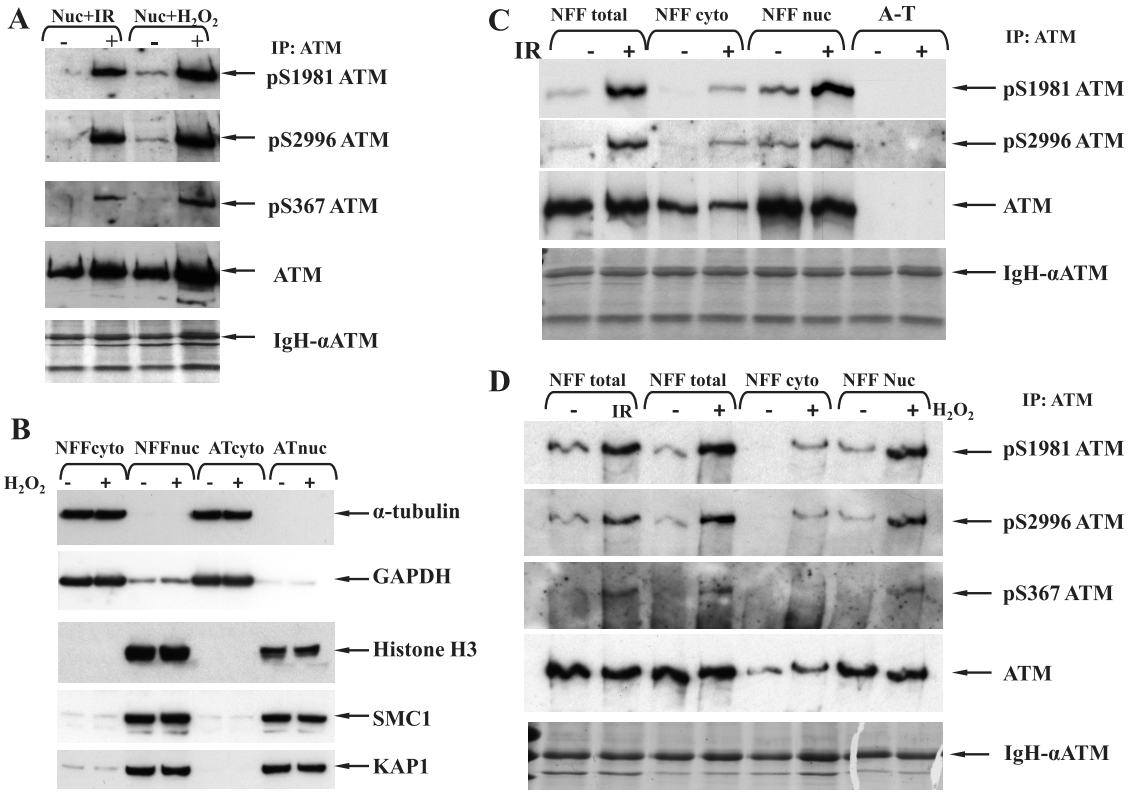

FIG. 1. **ATM kinase activation by ionizing radiation (IR) and H_2O_2 in subcellular fractions. Normal human fibroblasts (NFF) were irradiated with 6 Gy or treated with 0.5 mM H_2O_2. NFF and A-T fibroblasts total, cytoplasmic, and nuclear extracts were prepared as described in the Methods and immunoprecipitated with anti-ATM antibody. Immunoprecipitated ATM was resolved on biphasic 5%/12% SDS-Polyacrylamide gel and Western blotting was performed with phospho-specific ATM antibodies. Variation in total ATM protein levels represents the different amount of ATM kinase present in subcellular fractions after immunoprecipitation.** (*A*) ATM kinase activation by ionizing radiation (IR) and H_2O_2 in nuclear fractions prepared from normal human fibroblasts (NFF). Activation was determined by ATM autophosphorylation using antibodies against different active forms. (*B*) Monitoring of subcellular fractionation using specific markers. Cytoplasmic proteins: tubulin and GAPDH; Nuclear proteins: histone H3, SMC1, and KAP1 (*C*) Active ATM kinase is detected in total extracts, nuclear and cytoplasmic fractions from NFF using phospho-specific antibodies against ATM. (*D*) ATM kinase activation induced either by IR or H_2O_2 in total cell extracts, cytoplasmic and nuclear extracts.

ionizing radiation (IR) at a number of different sites (6, 7) and S1981 by oxidative stress (9). We initially compared ATM autophosphorylation in nuclear extracts after exposure of primary neonatal foreskin fibroblasts (NFFs) to IR and oxidative stress (H_2O_2 treatment). Detection of similarly increased phosphorylation at Ser^{1981}, Ser^{2996}, and Ser^{367} by site-specific antibodies demonstrated that both agents induce activation of ATM via multi-site autophosphorylation (Fig. 1*A*). To monitor the purity of nuclear and cytoplasmic fractions, we carried out immunoblotting for a number of proteins from each compartment (Fig. 1*B*). Under these conditions both H_2O_2- and IR-induced γH2AX foci both in control and A-T fibroblasts (Supplemental Fig. 1).

Oxidative Stress and Ionizing Radiation Activate Cytoplasmic ATM—It is well established that the bulk of ATM protein is present in the nucleus, but the presence of cytoplasmic ATM has been reported in some cell types (29, 40). To address this, we initially determined whether cytoplasmic ATM was activated by IR. The results in Fig. 1*C* revealed that cytoplasmic ATM was activated by IR as determined by phosphorylation on Ser^{1981} and Ser^{2996}. The amount of activity was ~25% of that observed with nuclear ATM. This is in agreement with the relative amounts of ATM protein in the nucleus and cytoplasm. We then determined whether H_2O_2 could also activate ATM in both the nucleus and in the cytoplasm of primary control fibroblasts. We observed robust activation of ATM, as determined by phosphorylation of Ser^{1981} in total cell extracts (Fig. 1*D*). The bulk of this activation was observed in nuclear extracts; however, activation was also clearly detectable in the cytoplasmic fraction. The extent of activation by H_2O_2 was comparable to exposure to IR (Fig. 1*C* and Fig. 1*D*). Similarly, increased phosphorylation was observed for Ser^{2996} and Ser^{367}, both of which have been shown to be functionally important for ATM activation by DNA damage (8).

We have previously employed stable isotope dimethyl labeling to quantitate the relative change in abundance of ATM phosphorylation sites after stimulus by IR (8). We employed the same approach here to compare untreated and H_2O_2-treated cells. Similar to the detection of increased phosphor-

ylation by phosphosite-specific antibodies (Fig. 1*D*), we observed increased phosphorylation at Ser^{1981}, Ser^{367}, and Ser^{2996} following H_2O_2 treatment of both lymphoblastoid cells and fibroblasts (Supplemental Fig. 2). IR nonresponsive ATM site, Thr^{1885} (8) was similarly nonresponsive after H_2O_2 treatment. Thus, cytoplasmic ATM is autophosphorylated at three major sites following H_2O_2 treatment, and these sites are associated with ATM activation.

Activation of Additional Phosphoinositide-3-Like Kinases and Downstream Substrates—The three phosphoinositide-3-like kinases (PIKK), ATM, ATR, and DNA-PK, are all DNA damage response proteins and have overlapping substrate phosphorylation motifs (S/T)Q (51). Apart from ATM, other PIKK family members might be involved in the response to oxidative stress. To determine if other PIKK members are activated by H_2O_2, we monitored their activation and signaling alongside ATM in control fibroblasts and compared these results with A-T fibroblasts. Autophosphorylation of ATR on Ser^{428} was detected in control fibroblasts after IR and H_2O_2 treatment but not in A-T fibroblasts (Fig. 2*A*), indicating that it is potentially ATM dependent. Ser^{428} has been suggested to be a marker of ATR activation (67). Autophosphorylation on Ser^{2056} is an indicator of DNA-PK activation (68). Ser^{2056} phosphorylation was induced by H_2O_2 in both control and A-T fibroblasts (Fig. 2*A*), indicating its activation might be independent of ATM. The results in Fig. 2*B* outline downstream substrate signaling induced by IR and H_2O_2. It is evident from the absence of phosphorylation in A-T fibroblasts that the majority of these phosphorylations can be accounted for by ATM or ATR activation. On the other hand, it seems likely that ATM and DNA-PK could contribute to KAP1 phosphorylation. Thus, H_2O_2 treatment is likely to activate multiple PIKK family proteins. Overall, the data suggest ATM and ATR might be synergistically activated by H_2O_2 treatment, while DNA-PK signaling is likely to be independent of ATM. In support of this, activation of ATR and DNA-PK has already been reported (69, 70).

Identification of Potential Cytoplasmic ATM Substrates Following Oxidative Stress—To identify potential cytoplasmic ATM substrates and signaling pathways following H_2O_2 exposure, we performed a comparative phosphoproteomics experiment. As above, cytoplasmic extracts from untreated and H_2O_2-treated normal human fibroblasts were compared in four independent experiments. Additionally, cytoplasmic extracts from untreated and H_2O_2-treated A-T fibroblasts were compared in three independent experiments to aid in determining whether the observations in normal human fibroblasts are a result of ATM signaling. Quantitation of the differences between untreated and treated was enabled by duplex stable isotope dimethyl labeling (53, 54). Samples were analyzed by high-resolution mass spectrometry with an LTQ Orbitrap Velos, and the raw data were processed using MaxQuant (57). Phosphopeptide enrichment was performed utilizing the TiO2 -SIMAC -HILIC technique (56), which involves fractionation of

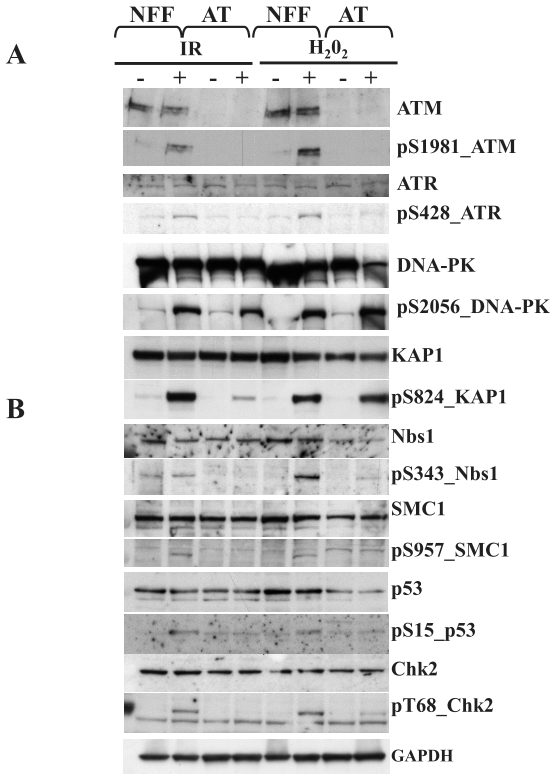

FIG. 2. (*A*) Activation of DNA damage response kinases by IR and H_2O_2 in normal human fibroblasts and A-T primary fibroblasts**.** Normal human fibroblasts (NFF) and A-T fibroblasts were irradiated with 6 Gy or treated with 0.5 mM H_2O_2. Total extracts were prepared as described in the Methods, and samples were run on NuPAGE 3–8% tris-acetate mini gels. Western blotting was performed with phospho-specific ATM, ATR, and DNA-PK antibodies as indicated. (*B*) ATM-dependent signaling in response to IR and H_2O_2 in normal human fibroblasts and A-T primary fibroblasts. Normal human fibroblasts (NFF) and A-T fibroblasts were irradiated with 6 Gy or treated with 0.5 mM H_2O_2. Total extracts were prepared as described in the Methods and samples were run on NuPAGE 4–12% Bis-Tris mini gels. Western blotting was performed with phospho-specific antibodies against known ATM substrates as indicated.

phosphopeptides via HILIC to increase the depth of phosphoproteome discovery. The strategy is outlined in Fig. 3*A*. Activation of ATM was confirmed for each biological replicate by monitoring the phosphorylation of known ATM substrates KAP1 and SMC1 by Western blotting of the normal human fibroblast lysates (Supplemental Fig. 3). ATM was reproducibly activated in each replicate.

A total of 9,833 phosphorylated sites were identified (8,763 unique), mapping to 2,716 proteins, at a false discovery rate of 1% at both the peptide and protein level (Supplemental Table I). A subset of these, 6,686, were high-confidence sites containing at least one site with a localization score ≥ 0.75 (Fig. 3*B* and Supplemental Table I), mapping to 2,536 unique proteins (Fig. 3*C*). The complete MaxQuant result files for the phosphopeptide identification and quantification are supplied as supplementary material. For normal human fibroblasts and A-T fibroblasts, preferential enrichment for cytoplasmic pro-

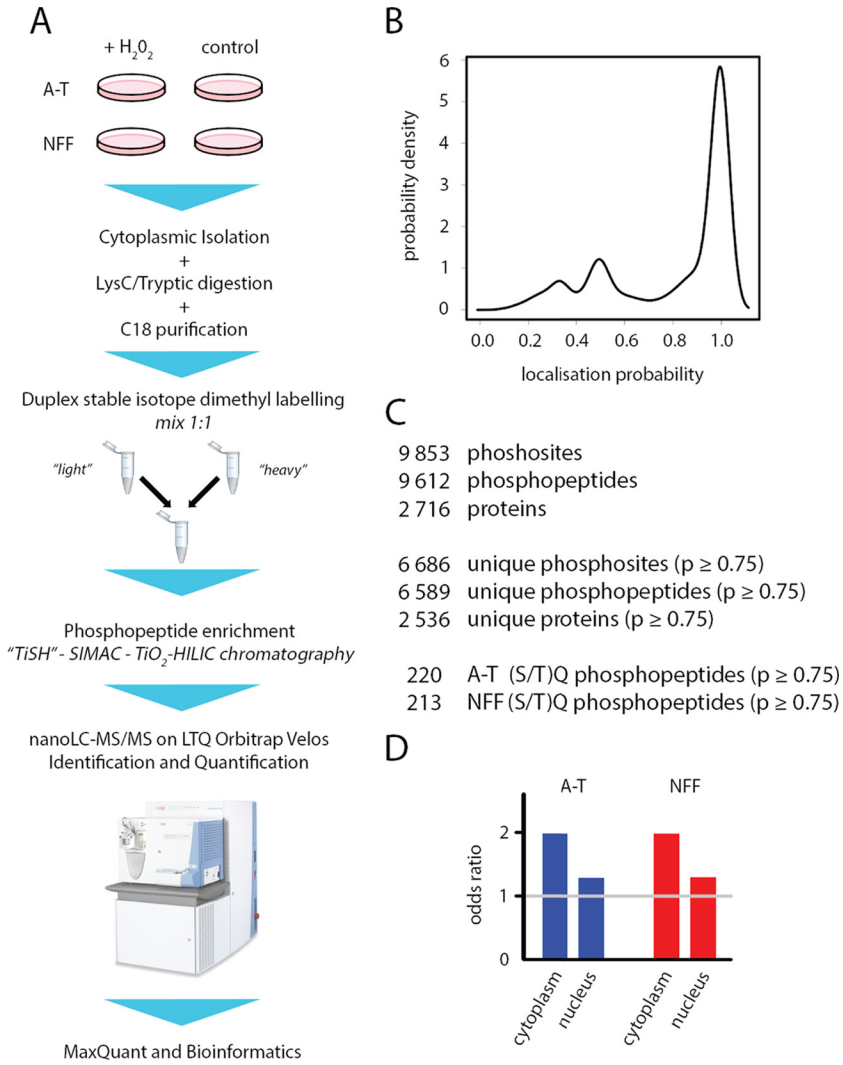

FIG. 3. **Phosphoproteomics workflow and identified phosphopeptides.** (*A*) Cultures of NFF and A-T cells were mock-treated or treated with H_2O_2. Cytoplasmic extracts of each were prepared, digested, and duplex stable isotope dimethyl labeled. Phosphopeptides were enriched and fractionated using the TiSH method and analyzed by LC-MS/MS. (*B*) Localization probability distribution of phosphosites identified using MaxQuant. (*C*) Counts of phosphopeptides and proteins at the thresholds used; p indicates localization probability. (*D*) Enrichment of cytoplasm and nucleus GO terms for the A-T and normal cells.

teins over nuclear proteins was observed (Fig. 3*D*). A subset of 213 and 220 phosphorylated peptides were in a (S/T)Q context in the normal human fibroblasts ($n = 4$) and A-T fibroblasts ($n = 3$), respectively; 203 were present in both normal and A-T (Fig. 3*C*). We compared all phosphorylated peptides that we identified to Beli *et al.* (25) since this is one of the few studies that captured cytoplasmic phosphopeptides in a DNA damage model. In total, Beli *et al.* identified 21,249 unique modified sequences, 11,776 and 13,177 for IR and etoposide, respectively. A relatively small number, 3,704 unique modified sequences, were in common between IR and etoposide. Of the total set 1,046 were in the p(S/T)Q context, 141 in common with IR and etoposide treatment. Of the 8,618 unique modified sequences (nonthresholded) in our dataset, 2,521 (29%) overlapped with those identified by Beli *et al.* (Supplemental Fig. 4*A*), 1,751 and 1,717 with IR and etoposide, respectively. We identified 321 unique p(S/T)Q-modified sequences in our complete data (H_2O_2 treated and untreated A-T and control data combined). Eighty-three (26%) of these unique phosphopeptides were also identified in the Beli *et al.* data set; IR (66) and etoposide (45) data set (Supplemental Fig. 4*B*).

The quantitative information for each high-confidence phosphopeptide was used to examine the changes in phosphopeptide abundance between the normal human fibroblasts and A-T fibroblasts following H_2O_2 treatment. This was done by extracting data sets that represent phosphorylated peptides identified as differentially or preferentially phosphorylated in each of the two cell types (normal human fibroblasts and A-T fibroblasts), resulting in four data sets (Fig. 4). Set 1

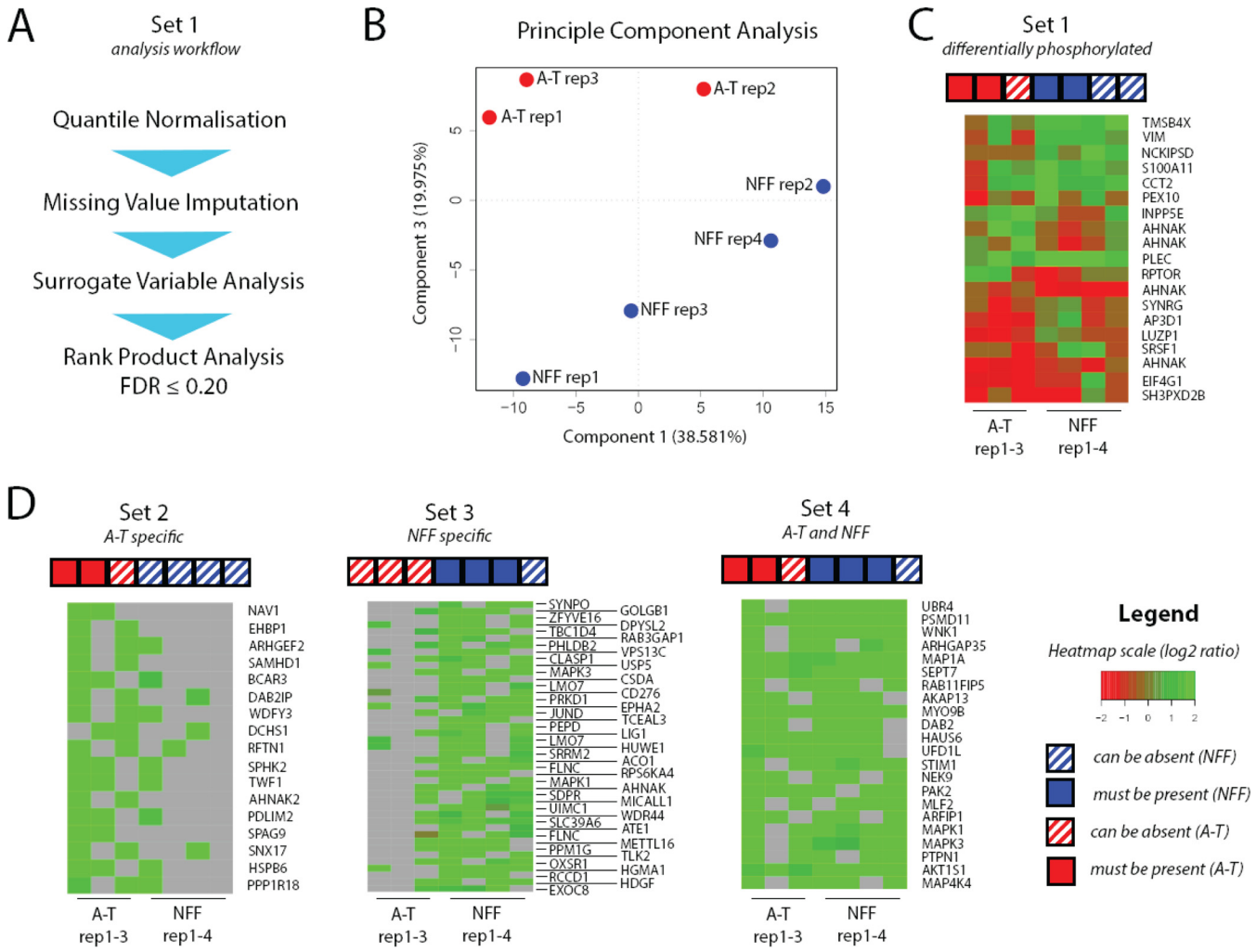

FIG. 4. **Analysis of phosphoproteomics data set by rank product statistics.** (*A*) Overview of normalization process for Set 1; quantile global normalization was followed by missing value imputation, surrogate variable analysis, and rank product analysis. (*B*) Principle component analysis projecting the first and third components of Set 1 data after normalization. (*C*) Heat map illustrating overall patterns for the peptides identified in Set 1. (*D*) Heat maps for Sets 2–4. The number of solid boxes indicates the number of times a phosphopeptide must be detected at to be included in the set. The number of boxes with diagonal lines indicates the number of times a that missing values for a particular phosphopeptide was permitted.

consisted of differentially phosphorylated peptides, *i.e.* peptides phosphorylated in both normal human fibroblasts and A-T fibroblasts but where the change in phosphorylation upon treatment with H_2O_2 differed. For Set 1 (Figs. 4*A*–4*C*), data were first normalized, missing values imputed, and surrogate variable analysis performed for suitability to a two-class rank product analysis. A clear separation and clustering of A-T from normal human fibroblasts was observed through application of unsupervised principle component analysis prior to rank product analysis (Fig. 4*B* and Supplemental Fig. 5). At a false discovery rate (FDR) threshold of 0.2 and employing 1,000 permutations to determine the FDR, we identified 19 peptides as differentially phosphorylated. These included 14 with increased phosphorylation in normal fibroblasts and five with decreased phosphorylation (Fig. 4*C*).

Sets 2 and 3 were allowed to have completely missing values for either normal or A-T fibroblasts, respectively, that is, the phosphopeptide was absent (*i.e.* not detected) in at least two replicates for both normal and A-T samples as per Set 1 inclusion criteria. Set 4 consisted of phosphopeptides that changed to a similar extent in both cells types, *i.e.* not differentially phosphorylated as per Set 1. Thus, these remaining sets were generated using a single class rank product analysis (FDR ≤ 0.2) to identify phosphopeptides specifically dysregulated by H_2O_2 in normal and/or A-T (Fig. 4*D*, *bottom* panel). Set 2 consisted of sites that changed preferentially in A-T fibroblasts, and 17 peptides fit this criterion. Set 3 consisted of phosphopeptides that preferentially changed in normal fibroblasts, and 43 fit this criterion. These latter peptides are most likely to contain potential ATM substrates because

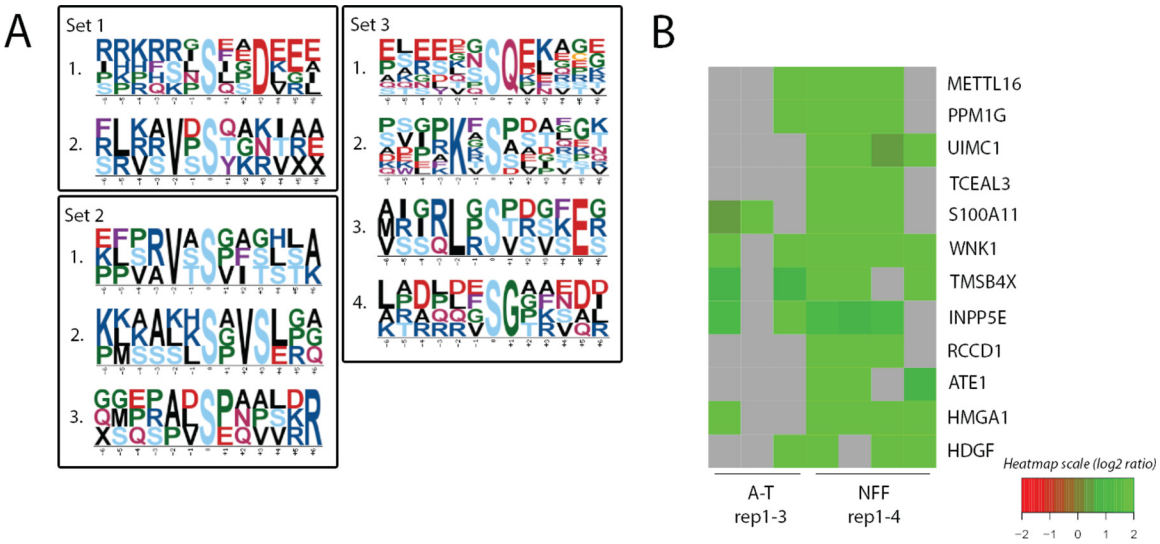

FIG. 5. **Potential protein kinase substrate motifs and regulated p(S/T)Q sites.** (*A*) MotifX analysis of Sets 1–3. (*B*) Heatmap showing $\log_2$ ratio values of p(S/T)Q containing phosphopeptides in Sets 1–4.

they were absent or not significantly changing in A-T fibroblasts. Set 4 consisted of phosphopeptides that changed in both control or A-T fibroblasts, and 22 of these peptides fit this criterion. This latter set is the least likely to contain ATM substrates because of the similar H_2O_2 response in ATM-defective cells. In summary, a total of 101 significantly regulated phosphopeptides were identified and classified as differentially or preferentially phosphorylated.

To confirm that the regulated phosphopeptides identified in these four sets were of cytoplasmic origin, we performed gene ontology (GO) analysis using the Database for Annotation Visualization and Integrated Discovery database (64) on the proteins containing the identified phosphorylation sites. Extraction of cytoplasm and nuclear terms revealed that the odds of the Set 1–4 proteins being associated with cytoplasmic terms was approximately twice the odds of being enriched for nuclear terms. Nuclear protein terms were close to null enrichment (approaching an odds ratio of 1) when compared with the background distribution (Supplemental Fig. 6*A*). Set 2 was not enriched for any GO terms, suggesting that there was not a consistent signature for the proteins harboring phosphosites in A-T only cells. Sets 1, 3, and 4 were each significantly enriched for the cytoplasm term (p values 0.023, 2.86E-05, and 4.83E-04, respectively) in contrast to the nuclear term (p values 0.633, 0.140, and 0.421, respectively) supporting cytoplasmic enrichment of our regulated phosphopeptide data.

We next performed motif enrichment analysis of modified sequences centered on the serine or threonine amino acid using Motif-x (65). The top motif for Set 1 was SXXD, indicating that these phosphopeptides might be substrates of an acidophilic protein kinase (Fig. 5*A*). The top motif identified for Set 3 was the consensus ATM substrate threonine glutamine sequence ($p < 0.01$) (Fig. 5*B*). No SQ sites were significantly overrepresented in Sets 2 or 4. No TQ sites were identified as significantly overrepresented. Annotation of all (S/T)Q-containing sequences identified three Set 1 phosphopeptides: Thr^{23} of thymosin $\beta 4$ and Ser^{101} of S100 calcium-binding protein A11 (S100A11) had increased phosphorylation and Ser^{99} of 72 kDa inositol polyphosphate 5-phosphatase had decreased phosphorylation in normal cells. Eight Set 3 (S/T)Q sites were also identified and will be discussed in greater detail below. Although Set 4 was not overrepresented in SQ motifs, a single SQ site at Ser^{167} of WNK lysine-deficient protein kinase 1 was identified and associated with increased phosphorylation.

Using an unbiased approach, we confirmed that predicted ATM substrates existed in the most relevant sets. Prediction of ATM targets from Set 1–4 phosphopeptide sequences was performed using NetPhosK (71), which uses neural network predictions. NetPhosK identified the greatest proportion of predicted ATM targets in Set 1 (21%) and Set 3 (23.4%), compared with Set 2 (0%) and Set 4 (0.05%) (Supplemental Fig. 6*B*). This was consistent with our ranked product analysis where we expected to find ATM targets in Set 1 and Set 3 preferentially.

Our experimental and bioinformatics approach therefore enabled us to narrow the reactive oxygen species phosphosignaling to (1) events occurring in, or preferentially in, normal cells but not in A-T cells, (Fig. 4, Set 1 and 3), (2) those significantly enriched for cytoplasm terms, and (3) those predicted to be ATM targets. In this narrow group, we observed 11 proteins phosphorylated at (S/T)Q sites. Of these, HMGA1, involved in p53 transcription regulation, is a previously described ATM substrate (72). UIMCI (RAP80), recruited to the sites of DNA double strand breaks, is also phosphorylated by ATM (73). Five other proteins, ATE1, METTL16, OSR1, PPM1G, and TCEAL3, have been identified in phosphopro-

teomic screens of the DNA damage response (21, 25, 26). A non-(S/T)Q site of OSR1 was in Set 3 (Ser^{359}). Phospho-Ser^{427} was detected twice in normal cells but not in A-T cells. However, it was below our false discovery threshold. The four remaining candidates have not been described previously in DNA damage screens and potentially represent novel ATM-dependent signaling targets.

In order to establish the signaling pathways affected by ROS, we performed network analysis using Ingenuity Pathway Analysis (IPA, Qiagen) and STRING (74), incorporating candidates identified from Sets 1–4 (Fig. 4). A summary of pathways impacted on appears in Supplemental Fig. 7. ROS is known to activate MAPK and PI3K/AKT signaling (75). Activation of these pathways was evident by changes to the abundance of phosphosites of Set 4 proteins Nck-interacting kinase (*MAP4K4*), MAPK1/ERK2, and MAPK3/ERK1, PRAS40 (*AKT1S1*), and to Set 1 protein RPTOR. Substrates of ATM and network neighbors are shown (Supplemental Fig. 7), predominantly arising from Set 3. A small cluster of these proteins are involved in ubiquitin-mediated protein degradation (ATE1, UREB1 (*HUWE1*), and UFD1L).

Validation of Candidate (S/T)Q Phosphosite Proteins—We selected several candidates from Set 1 and Set 3 showing up-regulation of phosphorylation on (S/T)Q motifs (see Fig. 5). Since no phospho-specific antibodies were available against the identified sites on these proteins, we carried out protein immunoprecipitation with an antibodies recognizing the ATM/ATR substrate motif p(S/T)Q followed by immunoblotting for the specific protein. Increased phosphorylation of the candidate protein OSR1 was detected in response to H_2O_2 treatment (Fig. 6*A*), which we attribute to the Ser^{427} phosphosite since it is in an SQ context. Under these conditions, we did not observe induced phosphorylation of this protein in A-T fibroblasts. Furthermore, IR (3Gy) failed to induce OSR1 phosphorylation, implying a H_2O_2-specific phosphorylation of OSR1. H_2O_2-induced phosphorylation of two known substrates of ATM (Mre11 and Rad50) was also observed (Fig. 6*A*). Similarly, H_2O_2-induced phosphorylation of two other candidate proteins, HDGF and ccdc82 (Fig. 6*A*). Semi-quantitative analysis revealed that HDGF was induced ~5.3-fold compared with twofold in A-T cells. These differences in phosphorylation follow the pattern observed in the MaxQuant analysis (Supplemental Table I). In the case of ccdc82, the increases were ~2.5-fold and 1.5-fold, respectively, again reflecting what was observed in the MS analysis; however, this particular candidate was only detected twice in NFF and therefore did not meet our stringent Set 3 criteria. Reduced phosphorylation of these proteins was observed in A-T fibroblasts. A number of available antibodies against other candidate proteins containing p(S/T)Q sites (ATE1, METTL16, TCEAL3, ATXN3, SNX17, MON1) were tested by immunoblotting and IF microscopy but failed to demonstrate changes in phosphorylation status or subcellular localization of these proteins (data not shown).

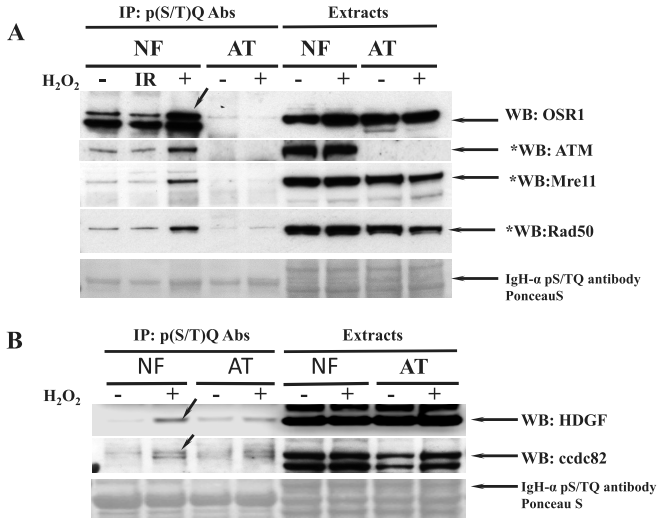

FIG. 6. **Detection of candidate proteins from phosphoproteomics screen in phospho-(S/T)Q ATM/ATR substrate antibody immunoprecipitates. Extracts from untreated, irradiated (3 Gy) and hydrogen-peroxide-treated normal human fibroblasts (NFF) and A-T fibroblasts were prepared as described in the Methods and immunoprecipitated with p-(S/T)Q ATM/ATR substrate antibodies. Immunoprecipitates and extracts were run on 4–12% NuPage gels and gels were transferred to nitrocellulose membrane and stained with Ponceau S to estimate the loading. Western blotting was performed with antibodies against a selection of candidate proteins from the phosphoproteomics screen.** listtext(A) (*B*) HDGF and ccdc82. * Western blotting with antibodies against known substrates of ATM kinase (Mre11, Rad50) was performed to access the efficiency of p(S/T)Q antibodies imunnoprecipitations.

Phosphorylation of S100A11 protein was also confirmed to be ATM dependent in this study. S100A11 is a cytoplasmic protein, involved in Ca^{2+} signaling (76). This protein was previously shown to be translocated to the nucleus by PKCα-mediated phosphorylation in response to transforming growth factor β treatment (77). We also observed diffuse cytoplasmic staining for S100A11 in NFF cells that translocated to the nucleus in response to H_2O_2 treatment (Fig. 7*A*). S100A11 was also localized to the cytoplasm in A-T fibroblasts, but the distribution was more perinuclear compared with NFF fibroblasts and it failed to be translocated to the nucleus after H_2O_2 treatment. Colocalization was not observed with an early endosome marker, EEA1. Translocation of S100A11 under conditions that detect formation of H_2O_2-induced γH2AX foci by immunofluorescence microscopy demonstrated that nuclear staining of S100A11 did not coincide with DNA damage foci (Fig. 7*B*).

DISCUSSION

ATM plays a central role in the response to DNA double strand breaks, phosphorylating upwards of 700 substrates that are involved in a variety of cellular processes that include cell cycle control, DNA repair, transcription, apoptosis, and cell proliferation (4). However, it is now evident that ATM is also activated by other DNA-damaging agents, chromatin

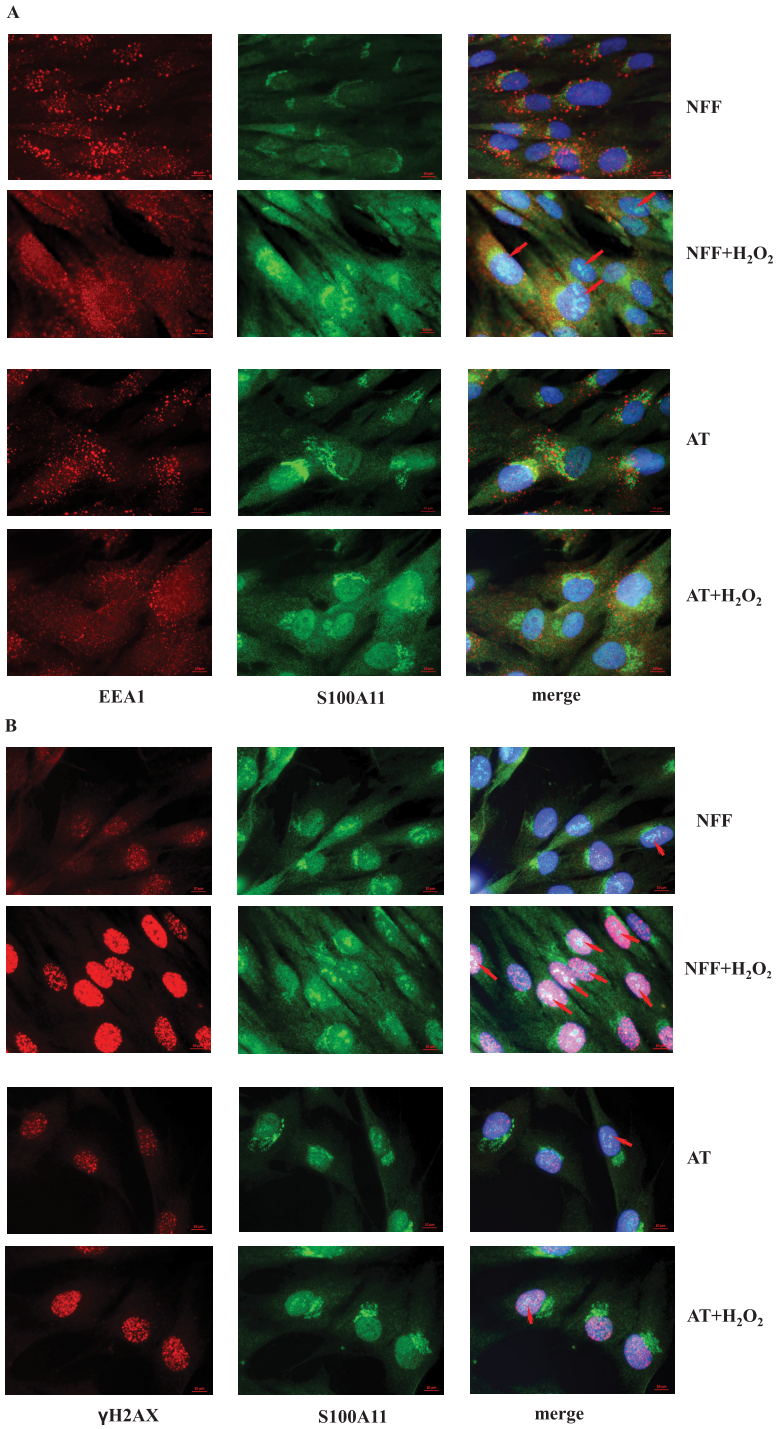

FIG. 7. **Translocation of S100A11 to the nucleus in response to H_2O_2 treatment is defective in A-T fibroblasts.** Normal control fibroblasts (NFF) and A-T fibroblasts were grown on coverslips, treated with hydrogen peroxide, or left untreated as described in the Methods. IF microscopy was performed using antibodies against EEA1 and S100A11 (*A*) or γH2AX and S100A11 (*B*). Cells were imaged on a Zeiss AxioImager M1 fluorescent microscope using x63 oil lens. Images were taken with an Axiocam503 mono camera and processed using ZEN software (Zeiss). Separate channels and merged images are shown. The scale bar is 10 μM.

modification and by oxidative stress not involving damage to DNA (9). In order to elucidate the pathways activated by the different agents, it is important to identify the substrates that mediate the various effects. In the present study, we employed oxidative stress (H_2O_2) to identify proteins phosphorylated by ATM with a view to understanding the defective phenotype in A-T. We selected a concentration of H_2O_2 that lead to elevated ATM activation in both the nucleus and cytoplasm.

The presence of ATM in the cytoplasm is in keeping with previous reports for a number of different cells including postmitotic cells (11, 28, 29, 38). While a number of cytoplasmic proteins have been shown to be phosphorylated after ATM activation by DNA-damaging agents (28, 42–50), the only direct evidence for activation in the cytoplasm has only recently been demonstrated (10). In that report, they show that ATM is localized to the peroxisome in agreement with earlier observations (11). They also show that ATM localized to the peroxisome via the import receptor PEX5. On exposure to ROS, ATM becomes activated to phosphorylate PEX5 at Ser^{140}, which leads to its ubiquitylation and subsequent binding to p62 to induce pexophagy. We did not detect PEX5 among the list of substrates phosphorylated by ATM, but we did observe phosphorylation of other peroxisomal proteins: PEX1 (SQ site), PEX10, PEX14, and PEX19.

Here, we have provided evidence that cytoplasmic ATM is activated by autophosphorylation on Ser^{1981} and additional sites (Ser^{367} and Ser^{2996}). ATM was shown to be present in the cytoplasm of different cell types, and cytoplasmic substrates were identified after DNA damage. However, it was not clear whether cytoplasmic ATM was functioning as a protein kinase. Furthermore, we have identified a number of cytoplasmic substrates after activation of ATM by oxidative stress.

We applied a quantitative phosphoproteomics analysis using a modified TiSH global phosphoproteomics approach (56) to identify proteins altered in their phosphorylation state in normal fibroblasts and A-T cells in response to oxidative damage. Contributions from other members of the PIKK family are difficult to rule out. However, our parallel screening in A-T cells allowed an additional level of classification of candidate ATM substrate phosphosites. For example, in Sets 1 and 3, we identified cytoplasmic proteins that are likely to be *bona fide* ATM/ATR substrates, along with sites not confined to the p(S/T)Q motif. This is all that not surprising since ATM was previously shown to phosphorylate sites other than (S/T)Q (23).

We identified a total of 9,833 phosphorylation sites, including 6,686 high-confidence sites. For subsequent bioinformatics analyses, results were divided into four data sets: those differentially phosphorylated in NFF and A-T fibroblasts (Set 1); those present preferentially in A-T cells (Set 2); those present preferentially in normal cells (Set 3); and those phosphorylated in both (Set 4). This approach enabled us to identify a 101 robustly regulated phosphopeptides for further analyses. Sets 1 and 3 were identified as preferentially enriched in ATM consensus (S/T)Q sites (51), using an unbiased method.

Of these 11 (S/T)Q sites identified in Set 1 and 3, two of the proteins, HMGA1 and UIMC1 (RAP80), had already been shown to be substrates for ATM in response to DNA damage (72, 73). The high mobility group protein, HMGA1, which plays a role in chromosomal organization, transcription regulation, and response to DNA damage, interacts with ATM and is a target for this kinase. HMGA1 is phosphorylated on Ser^{88} after DNA damage, but we observed ATM-dependent phosphorylation at a second site: Ser^{9}. Both sites are highly conserved in mammals. The ubiquitin interaction motif domain-containing protein, RAP80, has been shown to be a substrate for ATM Ser^{205} (73). Again, in this case, we identified a different site Ser^{101} of ATM-dependent phosphorylation. Of the remaining nine candidates identified, two, OSR1 and PPM1G, were identified in a previous phosphoproteomics screens after DNA damage (21, 25). The splicing-regulator phosphatase PPM1G was phosphorylated at Ser^{183} and Ser^{201}, both of which are PIKK sites. Where cells were treated with either etoposide or IR, PPM1G was recruited to DNA-damaged sites a short time after irradiation, but it was not reported whether phosphorylation at either of these sites influenced recruitment. PPM1G responded similarly to IR and etoposide in the Beli et al study.

We demonstrated that the oxidative stress responsive 1 protein (OSR1) was sixfold up-regulated in response to H_2O_2 treatment at a non-(S/T)Q site and 1.5-fold up-regulated at an (S/T)Q Ser^{427} site ($n = 2$), which was supported by p(S/T)Q-specific immunoblot analysis. Under these conditions, no induction was observed after IR treatment and failure to obtain an induction in A-T cells supports the ATM dependence of this phosphorylation. Previous data have shown that OSR1 is activated only by oxidative stress, notably sorbitol hypotonicity, and, to a lesser extent, NaCl (78). This protein kinase in turn has been shown to directly phosphorylate the N-terminal regulatory regions of calcium-chloride-transporters, including NKCCI, NKCC2, and NCC (79). However, since A-T is not characterized by channelopathy, it is possible that the response of OSR1 to oxidative stress is mediated through other undefined substrates, which might impact on other aspects of the A-T phenotype. An increased level of phosphorylation in response to H_2O_2 was observed for both HDGF and ccdc82 in control cells compared with A-T. HDGF, present in both the cytoplasm and nucleus, plays an important role in normal tissue development and is frequently overexpressed in cancer (80). It is not clear how phosphorylation affects the activity of this survival factor. Since ATM functions to protect against cancer (reviewed in (32)), it is possible that phosphorylation alters HDGF activity.

The cytoplasmic protein S100A11 showed a 3.3-fold (average) increase in phosphorylation in control *versus* A-T cells treated with H_2O_2. However, immunoblotting following immunoprecipitation with anti-p(S/T)Q motif antibody did not confirm the increase in phosphorylation detected using quantitative mass spectrometry. This is not too surprising since immunoprecipitation with anti-(S/T)Q antibody does not detect all known radiation-induced protein phosphorylations (our unpublished data). However, treatment of control cells with H_2O_2 caused S100A11 protein to relocalize from the cytoplasm to the nucleus in up to 60% of cells. On the other hand, the S100A11 was largely deficient in localizing to the

nucleus in A-T cells in response to H_2O_2. Overall, this suggests that S100A11 phosphorylation results in it being localized to the nucleus, and this is markedly reduced in A-T cells due to reduced phosphorylation in the absence of ATM.

S100A11 is a member of the S100 family of Ca^{2+}-binding proteins that are involved in cell cycle progression and signal transduction (81). Murzik *et al.* (82) have shown that Rad54B targeting to DNA double strand breaks requires complex formation with S100A11 implicating this protein in DNA repair. Furthermore, DNA damage involves a nucleolin-mediated translocation of S100A11 from the cytoplasm to the nucleus that is dependent on the phosphorylation activity of PKCα (83). It appears likely that this translocation of S100A11 into the nucleus may inhibit cell proliferation through increased levels of the cyclin kinase inhibitor p21 (84). S100A11 contains a single SQ site (Ser^{101}) close to the C terminus of the protein, which we demonstrated was phosphorylated to a greater extent in normal fibroblasts after H_2O_2 treatment. This suggests that ATM-dependent phosphorylation of S100A11 also controls its entry into the nucleus and perhaps involvement in DNA repair and response to oxidative stress. Further analysis was also carried out with other candidate substrates identified (ATE1, METTL16, TCEAL3, ATXN3, SNX17, and MON1) for which antibodies were available, but none showed evidence of increased phosphorylation or cellular redistribution (data not shown).

In summary, we have identified 2,716 proteins which demonstrated phosphorylation changes in response to oxidative damage in the cytoplasm. Of these, 43 were phosphorylated in normal fibroblasts but not in A-T cells, and a further 19 were differentially phosphorylated. These sets were enriched for the known (S/T)Q motif and predicted ATM targets. We validated phosphorylation changes for some of these proteins based on known function and relationship to the A-T phenotype. The challenge ahead is to confirm additional sites of phosphorylation and to investigate the effect of phosphorylation on function and how it impacts on the A-T phenotype.

Acknowledgments—We thank Aine Farell for excellent technical assistance. LTQ-Orbitrap Velos data were acquired at the Biomedical Proteomics and Australian Cancer Research Foundation (ACRF) Centre for Kinomics, Children's Medical Research Institute, Westmead, NSW 2145, Australia.

* This work was supported by grants from the National Health and Medical Research Council to M.F.L and M.E.G. M.F.L. received Fellowship support from the NHMRC. K.E.-K. is supported by the Lundbeck Foundation (Postdoctoral Fellowship), The Danish Council for Independent Research and the European Union FP7 Marie Curie Actions - COFUND program (MOBILEX Postdoctoral Fellowship DFF-1325-00154).

[S] This article contains supplemental material Supplemental Table I and Supplemental Figs. 1–7.

** To whom correspondence should be addressed Tel: +61 7 3346 6045; E-mail: m.lavin@uq.edu.au

REFERENCES

1. Lavin, M. F. (2008) Ataxia-telangiectasia: From a rare disorder to a paradigm for cell signalling and cancer. *Nat. Rev. Mol. Cell Biol.* **9,** 759–769
2. Derheimer, F. A., and Kastan, M. B. (2010) Multiple roles of ATM in monitoring and maintaining DNA integrity. *FEBS Lett.* **584,** 3675–3681
3. Shiloh, Y. (2014) ATM: Expanding roles as a chief guardian of genome stability. *Exp. Cell Res.* **329,** 154–161
4. Shiloh, Y., and Ziv, Y. (2013) The ATM protein kinase: Regulating the cellular response to genotoxic stress, and more. *Nat. Rev. Mol. Cell Biol.* **14,** 197–210
5. Paull, T. T. (2015) Mechanisms of ATM activation. *Annu. Rev. Biochem.* **84,** 711–738
6. Bakkenist, C. J., and Kastan, M. B. (2003) DNA damage activates ATM through intermolecular autophosphorylation and dimer dissociation. *Nature* **421,** 499–506
7. Kozlov, S. V., Graham, M. E., Peng, C., Chen, P., Robinson, P. J., and Lavin, M. F. (2006) Involvement of novel autophosphorylation sites in ATM activation. *EMBO J.* **25,** 3504–3514
8. Kozlov, S. V., Graham, M. E., Jakob, B., Tobias, F., Kijas, A. W., Tanuji, M., Chen, P., Robinson, P. J., Taucher-Scholz, G., Suzuki, K., So, S., Chen, D., and Lavin, M. F. (2011) Autophosphorylation and ATM activation: additional sites add to the complexity. *J. Biol. Chem.* **286,** 9107–9119
9. Guo, Z., Kozlov, S., Lavin, M. F., Person, M. D., and Paull, T. T. (2010) ATM activation by oxidative stress. *Science* **330,** 517–521
10. Zhang, J., Tripathi, D. N., Jing, J., Alexander, A., Kim, J., Powell, R. T., Dere, R., Tait-Mulder, J., Lee, J. H., Paull, T. T., Pandita, R. K., Charaka, V. K., Pandita, T. K., Kastan, M. B., and Walker, C. L. (2015) ATM functions at the peroxisome to induce pexophagy in response to ROS. *Nat Cell Biol.* **17,** 1259–1269
11. Watters, D., Kedar, P., Spring, K., Bjorkman, J., Chen, P., Gatei, M., Birrell, G., Garrone, B., Srinivasa, P., Crane, D. I., and Lavin, M. F. (1999) Localization of a portion of extranuclear ATM to peroxisomes. *J. Biol. Chem.* **274,** 34277–34282
12. Stiff, T., Walker, S. A., Cerosaletti, K., Goodarzi, A. A., Petermann, E., Concannon, P., O'Driscoll, M., and Jeggo, P. A. (2006) ATR-dependent phosphorylation and activation of ATM in response to UV treatment or replication fork stalling. *EMBO J.* **25,** 5775–5782
13. Chen, B. P., Uematsu, N., Kobayashi, J., Lerenthal, Y., Krempler, A., Yajima, H., Löbrich, M., Shiloh, Y., and Chen, D. J. (2007) Ataxia telangiectasia mutated (ATM) is essential for DNA-PKcs phosphorylations at the Thr-2609 cluster upon DNA double strand break. *J. Biol. Chem.* **282,** 6582–6587
14. Lee, B. S., Gapud, E. J., Zhang, S., Dorsett, Y., Bredemeyer, A., George, R., Callen, E., Daniel, J. A., Osipovich, O., Oltz, E. M., Bassing, C. H., Nussenzweig, A., Lees-Miller, S., Hammel, M., Chen, B. P., and Sleckman, B. P. (2013) Functional intersection of ATM and DNA-dependent protein kinase catalytic subunit in coding end joining during V(D)J recombination. *Mol. Cell. Biol.* **33,** 3568–3579
15. Ali, A., Zhang, J., Bao, S., Liu, I., Otterness, D., Dean, N. M., Abraham, R. T., and Wang, X. F. (2004) Requirement of protein phosphatase 5 in DNA-damage-induced ATM activation. *Genes Dev.* **18,** 249–254
16. Goodarzi, A. A., Jonnalagadda, J. C., Douglas, P., Young, D., Ye, R., Moorhead, G. B., Lees-Miller, S. P., and Khanna, K. K. (2004) Autophosphorylation of ataxia-telangiectasia mutated is regulated by protein phosphatase 2A. *EMBO J.* **23,** 4451–4461
17. Shreeram, S., Demidov, O. N., Hee, W. K., Yamaguchi, H., Onishi, N., Kek, C., Timofeev, O. N., Dudgeon, C., Fornace, A. J., Anderson, C. W., Minami, Y., Appella, E., and Bulavin, D. V. (2006) Wip1 phosphatase modulates ATM-dependent signaling pathways. *Mol Cell* **23,** 757–764
18. Sun, Y., Jiang, X., Chen, S., Fernandes, N., and Price, B. D. (2005) A role for the Tip60 histone acetyltransferase in the acetylation and activation of ATM. *Proc. Natl. Acad. Sci. U.S.A.* **102,** 13182–13187
19. Kaidi, A., and Jackson, S. P. (2013) KAT5 tyrosine phosphorylation couples chromatin sensing to ATM signalling. *Nature* **498,** 70–74
20. Gupta, A., Sharma, G. G., Young, C. S., Agarwal, M., Smith, E. R., Paull, T. T., Lucchesi, J. C., Khanna, K. K., Ludwig, T., and Pandita, T. K. (2005) Involvement of human MOF in ATM function. *Mol. Cell. Biol.* **25,** 5292–5305
21. Matsuoka, S., Ballif, B. A., Smogorzewska, A., McDonald, E. R., 3rd, Hurov, K. E., Luo, J., Bakalarski, C. E., Zhao, Z., Solimini, N., Lerenthal, Y., Shiloh, Y., Gygi, S. P., and Elledge, S. J. (2007) ATM and ATR substrate analysis reveals extensive protein networks responsive to DNA damage. *Science* **316,** 1160–1166
22. Mu, J. J., Wang, Y., Luo, H., Leng, M., Zhang, J., Yang, T., Besusso, D.,

Jung, S. Y., and Qin, J. (2007) A proteomic analysis of ataxia telangiectasia-mutated (ATM)/ATM-Rad3-related (ATR) substrates identifies the ubiquitin-proteasome system as a regulator for DNA damage checkpoints. *J. Biol. Chem.* **282,** 17330–17334
23. Bensimon, A., Schmidt, A., Ziv, Y., Elkon, R., Wang, S. Y., Chen, D. J., Aebersold, R., and Shiloh, Y. (2010) ATM-dependent and -independent dynamics of the nuclear phosphoproteome after DNA damage. *Sci. Signal* **3,** rs3
24. Choi, S., Srivas, R., Fu, K. Y., Hood, B. L., Dost, B., Gibson, G. A., Watkins, S. C., Van Houten, B., Bandeira, N., Conrads, T. P., Ideker, T., and Bakkenist, C. J. (2012) Quantitative proteomics reveal ATM kinase-dependent exchange in DNA damage response complexes. *J Proteome Res* **11,** 4983–4991
25. Beli, P., Lukashchuk, N., Wagner, S. A., Weinert, B. T., Olsen, J. V., Baskcomb, L., Mann, M., Jackson, S. P., and Choudhary, C. (2012) Proteomic investigations reveal a role for RNA processing factor THRAP3 in the DNA damage response. *Mol Cell* **46,** 212–225
26. Bennetzen, M. V., Larsen, D. H., Bunkenborg, J., Bartek, J., Lukas, J., and Andersen, J. S. (2010) Site-specific phosphorylation dynamics of the nuclear proteome during the DNA damage response. *Mol. Cell. Proteomics* **9,** 1314–1323
27. Olsen, J. V., Vermeulen, M., Santamaria, A., Kumar, C., Miller, M. L., Jensen, L. J., Gnad, F., Cox, J., Jensen, T. S., Nigg, E. A., Brunak, S., and Mann, M. (2010) Quantitative phosphoproteomics reveals widespread full phosphorylation site occupancy during mitosis. *Sci. Signal* **3,** ra3
28. Lim, D. S., Kirsch, D. G., Canman, C. E., Ahn, J. H., Ziv, Y., Newman, L. S., Darnell, R. B., Shiloh, Y., and Kastan, M. B. (1998) ATM binds to beta-adaptin in cytoplasmic vesicles. *Proc. Natl. Acad. Sci. U.S.A.* **95,** 10146–10151
29. Barlow, C., Ribaut-Barassin, C., Zwingman, T. A., Pope, A. J., Brown, K. D., Owens, J. W., Larson, D., Harrington, E. A., Haeberle, A. M., Mariani, J., Eckhaus, M., Herrup, K., Bailly, Y., and Wynshaw-Boris, A. (2000) ATM is a cytoplasmic protein in mouse brain required to prevent lysosomal accumulation. *Proc. Natl. Acad. Sci. U.S.A.* **97,** 871–876
30. Alexander, A., and Walker, C. L. (2010) Differential localization of ATM is correlated with activation of distinct downstream signaling pathways. *Cell Cycle* **9,** 3685–3686
31. Bhatti, S., Kozlov, S., Farooqi, A. A., Naqi, A., Lavin, M., and Khanna, K. K. (2011) ATM protein kinase: The linchpin of cellular defenses to stress. *Cell Mol. Life Sci.* **68,** 2977–3006
32. Stagni, V., Oropallo, V., Fianco, G., Antonelli, M., Cinà, I., and Barilà, D. (2014) Tug of war between survival and death: Exploring ATM function in cancer. *Int. J. Mol. Sci.* **15,** 5388–5409
33. Barzilai, A., Rotman, G., and Shiloh, Y. (2002) ATM deficiency and oxidative stress: A new dimension of defective response to DNA damage. *DNA Repair* **1,** 3–25
34. Biton, S., Dar, I., Mittelman, L., Pereg, Y., Barzilai, A., and Shiloh, Y. (2006) Nuclear ataxia-telangiectasia mutated (ATM) mediates the cellular response to DNA double strand breaks in human neuron-like cells. *J. Biol. Chem.* **281,** 17482–17491
35. Kim, T. S., Kawaguchi, M., Suzuki, M., Jung, C. G., Asai, K., Shibamoto, Y., Lavin, M. F., Khanna, K. K., and Miura, Y. (2010) The ZFHX3 (ATBF1) transcription factor induces PDGFRB, which activates ATM in the cytoplasm to protect cerebellar neurons from oxidative stress. *Dis. Model Mech.* **3,** 752–762
36. Lee, J. H., Guo, Z., Myler, L. R., Zheng, S., and Paull, T. T. (2014) Direct activation of ATM by resveratrol under oxidizing conditions. *PLoS ONE* **9,** e97969
37. Bennetzen, M. V., Mariño, G., Pultz, D., Morselli, E., Faergeman, N. J., Kroemer, G., and Andersen, J. S. (2012) Phosphoproteomic analysis of cells treated with longevity-related autophagy inducers. *Cell Cycle* **11,** 1827–1840
38. Alexander, A., Cai, S. L., Kim, J., Nanez, A., Sahin, M., MacLean, K. H., Inoki, K., Guan, K. L., Shen, J., Person, M. D., Kusewitt, D., Mills, G. B., Kastan, M. B., and Walker, C. L. (2010) ATM signals to TSC2 in the cytoplasm to regulate mTORC1 in response to ROS. *Proc. Natl. Acad. Sci. U.S.A.* **107,** 4153–4158
39. Kuljis, R. O., Chen, G., Lee, E. Y., Aguila, M. C., and Xu, Y. (1999) ATM immunolocalization in mouse neuronal endosomes: Implications for ataxia-telangiectasia. *Brain Res* **842,** 351–358
40. Watters, D., Khanna, K. K., Beamish, H., Birrell, G., Spring, K., Kedar, P., Gatei, M., Stenzel, D., Hobson, K., Kozlov, S., Zhang, N., Farrell, A., Ramsay, J., Gatti, R., and Lavin, M. (1997) Cellular localisation of the ataxia-telangiectasia (ATM) gene product and discrimination between mutated and normal forms. *Oncogene* **14,** 1911–1921
41. Valentin-Vega, Y. A., Maclean, K. H., Tait-Mulder, J., Milasta, S., Steeves, M., Dorsey, F. C., Cleveland, J. L., Green, D. R., and Kastan, M. B. (2012) Mitochondrial dysfunction in ataxia-telangiectasia. *Blood* **119,** 1490–1500
42. Yang, D. Q., and Kastan, M. B. (2000) Participation of ATM in insulin signalling through phosphorylation of eIF-4E-binding protein 1. *Nat Cell Biol.* **2,** 893–898
43. Shouse, G. P., Nobumori, Y., Panowicz, M. J., and Liu, X. (2011) ATM-mediated phosphorylation activates the tumor-suppressive function of B56gamma-PP2A. *Oncogene* **30,** 3755–3765
44. Sapkota, G. P., Deak, M., Kieloch, A., Morrice, N., Goodarzi, A. A., Smythe, C., Shiloh, Y., Lees-Miller, S. P., and Alessi, D. R. (2002) Ionizing radiation induces ataxia telangiectasia mutated kinase (ATM)-mediated phosphorylation of LKB1/STK11 at Thr-366. *Biochem. J.* **368,** 507–516
45. Viniegra, J. G., Martínez, N., Modirassari, P., Hernández Losa, J., Parada Cobo, C., Sánchez-Arévalo Lobo, V. J., Aceves Luquero, C. I., Alvarez-Vallina, L., Ramón y Cajal, S., Rojas, J. M., and Sánchez-Prieto, R. (2005) Full activation of PKB/Akt in response to insulin or ionizing radiation is mediated through ATM. *J. Biol. Chem.* **280,** 4029–4036
46. Wu, Z. H., Wong, E. T., Shi, Y., Niu, J., Chen, Z., Miyamoto, S., and Tergaonkar, V. (2010) ATM- and NEMO-dependent ELKS ubiquitination coordinates TAK1-mediated IKK activation in response to genotoxic stress. *Mol. Cell* **40,** 75–86
47. Hinz, M., Stilmann, M., Arslan, S. Ç., Khanna, K. K., Dittmar, G., and Scheidereit, C. (2010) A cytoplasmic ATM-TRAF6-cIAP1 module links nuclear DNA damage signaling to ubiquitin-mediated NF-kappaB activation. *Mol. Cell* **40,** 63–74
48. Cosentino, C., Grieco, D., and Costanzo, V. (2011) ATM activates the pentose phosphate pathway promoting anti-oxidant defence and DNA repair. *EMBO J.* **30,** 546–555
49. Cam, H., Easton, J. B., High, A., and Houghton, P. J. (2010) mTORC1 signaling under hypoxic conditions is controlled by ATM-dependent phosphorylation of HIF-1alpha. *Mol Cell* **40,** 509–520
50. Li, J., Han, Y. R., Plummer, M. R., and Herrup, K. (2009) Cytoplasmic ATM in neurons modulates synaptic function. *Curr. Biol.* **19,** 2091–2096
51. Kim, S. T., Lim, D. S., Canman, C. E., and Kastan, M. B. (1999) Substrate specificities and identification of putative substrates of ATM kinase family members. *J. Biol. Chem.* **274,** 37538–37543
52. Maulucci, G., Labate, V., Mele, M., Panieri, E., Arcovito, G., Galeotti, T., Østergaard, H., Winther, J. R., De Spirito, M., and Pani, G. (2008) High-resolution imaging of redox signaling in live cells through an oxidation-sensitive yellow fluorescent protein. *Sci. Signal* **1,** pl3
53. Boersema, P. J., Raijmakers, R., Lemeer, S., Mohammed, S., and Heck, A. J. (2009) Multiplex peptide stable isotope dimethyl labeling for quantitative proteomics. *Nat. Protoc.* **4,** 484–494
54. Hsu, J. L., Huang, S. Y., Chow, N. H., and Chen, S. H. (2003) Stable-isotope dimethyl labeling for quantitative proteomics. *Anal. Chem.* **75,** 6843–6852
55. Thingholm, T. E., Jensen, O. N., Robinson, P. J., and Larsen, M. R. (2008) SIMAC (sequential elution from IMAC), a phosphoproteomics strategy for the rapid separation of monophosphorylated from multiply phosphorylated peptides. *Mol. Cell. Proteomics* **7,** 661–671
56. Engholm-Keller, K., Birck, P., Størling, J., Pociot, F., Mandrup-Poulsen, T., and Larsen, M. R. (2012) TiSH—A robust and sensitive global phosphoproteomics strategy employing a combination of TiO2, SIMAC, and HILIC. *J. Proteomics* **75,** 5749–5761
57. Cox, J., and Mann, M. (2008) MaxQuant enables high peptide identification rates, individualized p.p.b.-range mass accuracies and proteome-wide protein quantification. *Nat. Biotechnol.* **26,** 1367–1372
58. Vizcaíno, J. A., Deutsch, E. W., Wang, R., Csordas, A., Reisinger, F., Ríos, D., Dianes, J. A., Sun, Z., Farrah, T., Bandeira, N., Binz, P. A., Xenarios, I., Eisenacher, M., Mayer, G., Gatto, L., Campos, A., Chalkley, R. J., Kraus, H. J., Albar, J. P., Martinez-Bartolomé, S., Apweiler, R., Omenn, G. S., Martens, L., Jones, A. R., and Hermjakob, H. (2014) ProteomeXchange provides globally coordinated proteomics data submission and dissemination. *Nat. Biotechnol.* **32,** 223–226
59. Breitling, R., Armengaud, P., Amtmann, A., and Herzyk, P. (2004) Rank

products: A simple, yet powerful, new method to detect differentially regulated genes in replicated microarray experiments. *FEBS Lett.* **573,** 83–92
60. Bolstad, B. M., Irizarry, R. A., Astrand, M., and Speed, T. P. (2003) A comparison of normalization methods for high density oligonucleotide array data based on variance and bias. *Bioinformatics* **19,** 185–193
61. Troyanskaya, O., Cantor, M., Sherlock, G., Brown, P., Hastie, T., Tibshirani, R., Botstein, D., and Altman, R. B. (2001) Missing value estimation methods for DNA microarrays. *Bioinformatics* **17,** 520–525
62. Leek, J. T., and Storey, J. D. (2007) Capturing heterogeneity in gene expression studies by surrogate variable analysis. *PLoS Genet.* **3,** 1724–1735
63. Hong, F., Breitling, R., McEntee, C. W., Wittner, B. S., Nemhauser, J. L., and Chory, J. (2006) RankProd: A bioconductor package for detecting differentially expressed genes in meta-analysis. *Bioinformatics* **22,** 2825–2827
64. Huang da, W., Sherman, B. T., and Lempicki, R. A. (2009) Systematic and integrative **19131956**
65. Chou, M. F., and Schwartz, D. (2011) Biological sequence motif discovery using motif-x. *Curr. Protoc. Bioinformatics* **13,** Unit 13.15–24
66. Jenkins, C. W., and Xiong, Y. (1996) Immunoprecipitation and immunoblotting in cell cycle studies. In: Pagano, M., ed. *Cell Cycle-Materials and Methods*, pp. 250–264, Springer
67. Nam, E. A., Zhao, R., Glick, G. G., Bansbach, C. E., Friedman, D. B., and Cortez, D. (2011) Thr-1989 phosphorylation is a marker of active ataxia telangiectasia-mutated and Rad3-related (ATR) kinase. *J. Biol. Chem.* **286,** 28707–28714
68. Meek, K., Douglas, P., Cui, X., Ding, Q., and Lees-Miller, S. P. (2007) trans Autophosphorylation at DNA-dependent protein kinase's two major autophosphorylation site clusters facilitates end processing but not end joining. *Mol. Cell. Biol.* **27,** 3881–3890
69. Katsube, T., Mori, M., Tsuji, H., Shiomi, T., Wang, B., Liu, Q., Nenoi, M., and Onoda, M. (2014) Most hydrogen peroxide-induced histone H2AX phosphorylation is mediated by ATR and is not dependent on DNA double-strand breaks. *J. Biochem.* **156,** 85–95
70. Li, M., Lin, Y. F., Palchik, G. A., Matsunaga, S., Wang, D., and Chen, B. P. (2014) The catalytic subunit of DNA-dependent protein kinase is required for cellular resistance to oxidative stress independent of DNA double-strand break repair. *Free Radic. Biol. Med.* **76,** 278–285
71. Blom, N., Sicheritz-Pontén, T., Gupta, R., Gammeltoft, S., and Brunak, S. (2004) Prediction of post-translational glycosylation and phosphorylation of proteins from the amino acid sequence. *Proteomics* **4,** 1633–1649
72. Pentimalli, F., Palmieri, D., Pacelli, R., Garbi, C., Cesari, R., Martin, E., Pierantoni, G. M., Chieffi, P., Croce, C. M., Costanzo, V., Fedele, M., and Fusco, A. (2008) HMGA1 protein is a novel target of the ATM kinase. *Eur. J. Cancer* **44,** 2668–2679
73. Yan, J., Yang, X. P., Kim, Y. S., and Jetten, A. M. (2008) RAP80 responds to DNA damage induced by both ionizing radiation and UV irradiation and is phosphorylated at Ser 205. *Cancer Res.* **68,** 4269–4276
74. Szklarczyk, D., Franceschini, A., Wyder, S., Forslund, K., Heller, D., Huerta-Cepas, J., Simonovic, M., Roth, A., Santos, A., Tsafou, K. P., Kuhn, M., Bork, P., Jensen, L. J., and von Mering, C. (2015) STRING v10: Protein–protein interaction networks, integrated over the tree of life. *Nucleic Acids Res.* **43,** D447–D452
75. Finkel, T. (2011) Signal transduction by reactive oxygen species. *J. Cell Biol.* **194,** 7–15
76. He, H., Li, J., Weng, S., Li, M., and Yu, Y. (2009) S100A11: diverse function and pathology corresponding to different target proteins. *Cell Biochem. Biophys.* **55,** 117–126
77. Sakaguchi, M., Miyazaki, M., Sonegawa, H., Kashiwagi, M., Ohba, M., Kuroki, T., Namba, M., and Huh, N. H. (2004) PKCalpha mediates TGF-beta-induced growth inhibition of human keratinocytes via phosphorylation of S100C/A11. *J. Cell Biol.* **164,** 979–984
78. Chen, W., Yazicioglu, M., and Cobb, M. H. (2004) Characterization of OSR1, a member of the mammalian Ste20p/germinal center kinase subfamily. *J. Biol. Chem.* **279,** 11129–11136
79. Moriguchi, T., Urushiyama, S., Hisamoto, N., Iemura, S., Uchida, S., Natsume, T., Matsumoto, K., and Shibuya, H. (2005) WNK1 regulates phosphorylation of cation-chloride-coupled cotransporters via the STE20-related kinases, SPAK and OSR1. *J. Biol. Chem.* **280,** 42685–42693
80. Bao, C., Wang, J., Ma, W., Wang, X., and Cheng, Y. (2014) HDGF: A novel jack-of-all-trades in cancer. *Future Oncol.* **10,** 2675–2685
81. Foertsch, F., Teichmann, N., Kob, R., Hentschel, J., Laubscher, U., and Melle, C. (2013) S100A11 is involved in the regulation of the stability of cell cycle regulator p21(CIP1/WAF1) in human keratinocyte HaCaT cells. *FEBS J.* **280,** 3840–3853
82. Murzik, U., Hemmerich, P., Weidtkamp-Peters, S., Ulbricht, T., Bussen, W., Hentschel, J., von Eggeling, F., and Melle, C. (2008) Rad54B targeting to DNA double-strand break repair sites requires complex formation with S100A11. *Mol. Biol. Cell* **19,** 2926–2935
83. Gorsler, T., Murzik, U., Ulbricht, T., Hentschel, J., Hemmerich, P., and Melle, C. (2010) DNA damage-induced translocation of S100A11 into the nucleus regulates cell proliferation. *BMC Cell Biol.* **11,** 100
84. Gartel, A. L., and Tyner, A. L. (2002) The role of the cyclin-dependent kinase inhibitor p21 in apoptosis. *Mol. Cancer Ther.* **1,** 639–649